Hybrid Systems for Photovoltaic Thermal Regulation

Sertan Erdem

Submitted to the
Institute of Graduate Studies and Research
in partial fulfillment of the requirements for the degree of

Master of Science
in
Mechanical Engineering

Eastern Mediterranean University
February 2023
Gazimağusa, North Cyprus

Approval of the Institute of Graduate Studies and Research

Prof. Dr. Ali Hakan Ulusoy
Director

I certify that this thesis satisfies all the requirements as a thesis for the degree of Master of Science in Mechanical Engineering.

Assoc. Prof. Dr. Murat Özdenefe
Chair, Department of Mechanical Engineering

We certify that we have read this thesis and that in our opinion it is fully adequate in scope and quality as a thesis for the degree of Master of Science in Mechanical Engineering.

Assoc. Prof. Dr. Murat Özdenefe
Supervisor

Examining Committee

1. Prof. Dr. Uğur Atikol

2. Prof. Dr. Mustafa Dağbaşı

3. Assoc. Prof. Dr. Murat Özdenefe

ABSTRACT

The cost of photovoltaic (PV) panels has decreased significantly in recent years, making their use widespread in homes for generating electricity. Despite the fact that PVs rely on the free energy of the sun, they have low conversion efficiency. Moreover, their efficiency decreases as the temperature of the cells rises, which is inevitable under solar radiation.

The current study aims to find a solution to the previously mentioned problem by examining phase change material (PCM)-based passive hybrid cooling systems for reducing PV temperatures. This examination was done through an experimental approach. Four different hybrid cooling systems which incorporate various melting point PCMs (25°C and 35°C) along with different heat transfer elements (fins and porous medium) were manufactured and tested under laboratory conditions. The experiments measured the temperature of the PV panels, as well as the generated current and voltage. Results showed that the hybrid cooling system consisting of low melting point PCM and fins resulted in the greatest temperature drop of 17°C compared to the test case of a PV without any cooling system. The maximum efficiency increase was found to be 17% through experimental calculation and 7% through theoretical calculation, using the low melting point PCM and porous medium configuration. The results also indicated that configurations with low melting point PCM are effective when the environmental temperature is moderate.

Keywords: PCM-Based Hybrid Cooling Systems, PV Cooling, Photovoltaics, Thermal Regulation, Renewable Energy, Efficiency Increase.

ÖZ

Güneşten ışınları ile bedava enerji üretimine olanak tanıması ve son yıllardaki fiyat düşüşüyle evlerde enerji üretimi amacıyla kullanımı yaygınlaşan fotovoltaik (FV) panellerin ne yazık ki enerji verimliliği konusunda yetersiz oluşu su götürmez bir gerçektir. Buna ek olarak ise, FV verimliliği yükselen güneş hücre sıcaklıklarıyla daha da düşmektedir, ki bu durum güneş ışınlarından enerji üreten bir araç için kaçınılmazdır.

Bu çalışma, daha önceden bahsedilen sorunun çözümü için faz değiştiren malzeme (FDM) tabanlı pasif hibrit soğutma sistemlerinin kullanılmasını öneren deneysel bir çalışmadır. Laboratuvar ortamında iki farklı ergime sıcaklığı olan FDM (25°C ve 35°C) ve iki farklı ısı iletim elemanı (kanatçık ve gözenekli ortam) kullanılarak dört ayrı hibrit soğutma sistemi test edilmiştir. Deney süresi boyunca FV panel sıcaklıkları ile birlikte üretilen gerilim ve akım ölçülmüştür. Deney sonuçlarında düşük ergime sıcaklığına sahip FDM ve kanatçık kombinasyonun sadece FVnin olduğu kontrol durumuna göre anlık olarak 17°C daha soğuk kaldığı kaydedilmiştir. Buna ek olarak, düşük ergime sıcaklığına sahip FDM ve geçirgen ortam içeren durumun FV verimliliğini deneysel olarak %17 ve teorik olarak %7 seviyesinin üzerine çıkardığı hesaplanmıştır.

Anahtar Kelimeler: FDM Tabanlı Hibrit Soğutma Sistemleri, FV Soğutma, Fotovoltaik, Sıcaklık Kontrolü, Yenilenebilir Enerji, Verimlilik İyileştirmesi.

DEDICATION

To my family and my friends who became my family regardless of blood

ACKNOWLEDGMENT

I would like to thank my supervisor, Assoc. Prof. Dr. Murat Özdenefe, for his endless support and having an extra pair of eyes on my thesis. Although I would have tried my best to finish this study, it would not be this systematic without him. I am also grateful to Prof. Dr. Uğur Atikol for offering an opportunity for me to present my study in a seminar, that meant a lot to me.

I also would like to thank Dr. Cafer Kızılörs, Mr. Zafer Mulla (technician of Mechanical Engineering Department), Mr. Mehmet, Mr. Halit and Mr. Bilal (from EMU Technical Affairs), manufacturing process flowed a lot easier with their help. Additionally, I cannot ignore the emotional and physical support of my friend Mr. Oğuzhan Bozkurt. He was always there whenever I needed help.

I would also like to express my gratitude to my family, although words cannot fully encompass my appreciation. I am grateful to my grandparents who raised me and guided me towards a love of science. I am also thankful for my parents, who supported me and helped me get to where I am now. Their love, wisdom, and actions have shaped who I am today.

TABLE OF CONTENTS

LIST OF TABLES

LIST OF FIGURES

LIST OF SYMBOLS AND ABBREVIATIONS

A_{cell}	Solar Cell Area
G	Irradiation
I_{mp}	Maximum Power Current
I_{sc}	Short Circuit Current
I_t	Instantaneous Current
P_{max}	Maximum Power
P_{out}	Output Power
$P_{out,E}$	Experimental Output Power
$P_{out,T}$	Theoretical Output Power
T_{ref}	Reference PV Temperature
$T_{PV,t}$	Instantaneous PV Temperature
V_{mp}	Maximum Power Voltage
V_{oc}	Open Circuit Voltage
V_t	Instantaneous Voltage
β_{ref}	Reference Power Decrement per Unit Temperature
$\frac{\delta_D}{D}$	Inaccuracy of Data Acquisition Module
$\frac{\delta_{EP}}{EP}$	Inaccuracy of Experimental Power
$\frac{\delta_G}{G}$	Inaccuracy of Irradiation
$\frac{\delta_I}{I}$	Inaccuracy of Current
$\frac{\delta_P}{P}$	Inaccuracy of Pyranometer
$\frac{\delta_T}{T}$	Inaccuracy of Temperature
$\frac{\delta_{TC}}{TC}$	Inaccuracy of Thermocouple
$\frac{\delta_{TP}}{TP}$	Inaccuracy of Theoretical Power

$\frac{\delta_V}{V}$	Inaccuracy of Voltage
$\frac{\delta_{\eta_E}}{\eta_E}$	Inaccuracy of Experimental Efficiency
$\frac{\delta_{\eta_T}}{\eta_T}$	Inaccuracy of Theoretical Efficiency
η_E	Experimental Efficiency
η_{ref}	Reference Efficiency
η_T	Theoretical Efficiency
DC	Direct Current
NOCT	Nominal Operation Cell Temperature
PCM	Phase Change Material
PV	Photovoltaic
TR	Thermal Regulation

Chapter 1

INTRODUCTION

1.1 Background

Unceasing rise of greenhouse gas emissions primarily due to fossil fuel combustions are considered to be the main reason of the climate change. Climate change, along with the fluctuation in fossil fuel prices, has driven the development and implementation of renewable energy technologies. Over the past few decades, there has been a significant increase in the generation of electricity from renewable sources, as seen in Figure 1. This shift towards renewable energy sources is crucial to mitigate the negative impacts of climate change and promote sustainable energy solutions.

Generation of energy –or conversion from one form to another- is one of the challenging issues of the humankind. In today's world, harvesting green energy as efficient as possible has the same importance as the harvesting energy from renewable sources. The most common ways to decrease the dependency on fossil fuels in dwellings are photovoltaic (PV) panels, solar thermals, wind turbines, nuclear power plants and geothermal [1]. Throughout the years from 1990 to 2020, electricity generation from renewables such as hydropower, biomass, geothermal, wind and solar increased more than threefold from 2.3 PWh to 7.4 PWh as it is shown in Figure 1 [2].

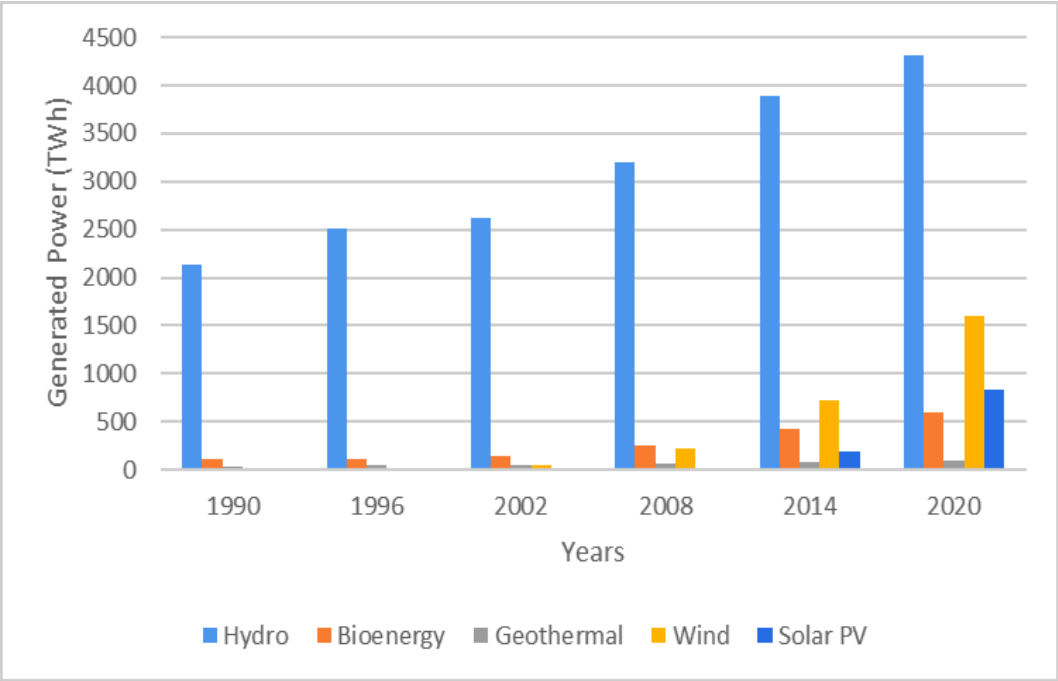

Figure 1: Renewable electricity generation based on generation technologies from 1990 to 2020 [2]

Today, harvesting solar energy for electricity production on site at homes by using PVs is prevalent, thanks to the fall of their prices during the past decades as it is visualized in Figure 2, ease in implementing the technology and abundance of solar energy available on various parts of the world. Although PVs are one of the widely used renewable energy generation technologies, they endure from low energy conversion efficiency –as low as converting about 18% of the incident radiation to electricity for commercial monocrystalline silicon solar cells- [3].

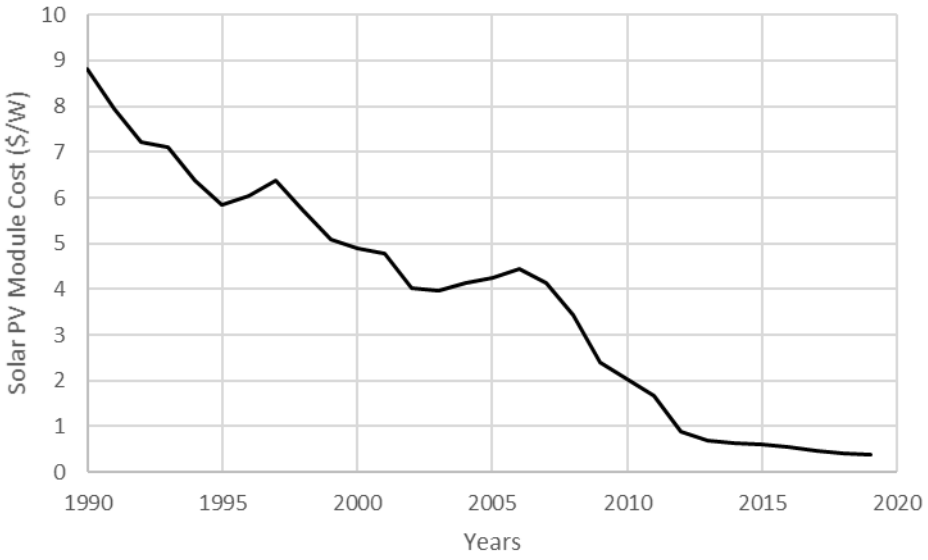

Figure 2: PV module costs per watt between 1990 and 2019 [4].

1.2 Problem Statement

PVs suffer from low efficiency. Their solar to electrical energy conversion efficiencies are about 25% in the best case scenario (for conventional PVs), meaning that only one fourth of the incident radiation can be converted to electrical energy [5,6]. In addition to their inherent low energy conversion efficiency, PVs experience decrease in efficiency with increase in their operational temperature. Based on various studies/manufacturers, operation temperatures above 25°C reduce electricity production of PV despite that the PVs usually reach high temperatures at times as high as 80°C under high insolation [7–9]. According to solar cell performance studies, photoelectric conversion efficiency decreases 0.4-0.65% per unit temperature increment [10–13]. In addition to negative impact on energy conversion efficiency, high temperatures are deteriorating PVs structural integrity.

In order to harvest maximum energy from PVs as well as to ensure longer operational life for them, thermal regulation (TR) can be considered as a solution. Two main

cooling techniques; active and passive cooling, prevail for thermally controlling PVs. Active cooling techniques can control the temperatures effectively by circulation of cooling fluids through conduits in contact with PV panels by means of pumps and fans, whereas fundamental heat transfer modes such as natural convection and conduction without any external energy use can be utilized for passive cooling approaches [14]. Numerous passive cooling techniques are applied to regulate the temperature of PV panels such as submerged water cooling, air flow induced by buoyancy, heat dissipaters or heat sinks, phase changing materials (PCMs), and evaporative cooling [15,16].

1.3 Objectives and Scope of the Study

The primary objective of this study is to investigate the TR of PVs with PCM-based passive hybrid cooling systems along with the energy conversion efficiency of PVs with and without passive hybrid TR systems through an experimental approach. It is also intended to investigate the increase in electricity generation due to the application of TR systems compared to the control case (Case 1) –thermally untreated PV–, and to reveal the system that would lead to the maximum power output.

Four different passive hybrid cooling systems will be investigated; i- fins integrated with low melting point (25°C peak) PCM (Case 2), ii- porous medium integrated with low melting point (25°C peak) PCM (Case 3), iii- fins integrated with high melting point (35°C peak) PCM (Case 4) and iv- porous medium integrated with high melting point (35°C peak) PCM (Case 2). TR systems will be realized by manufacturing the containers that will integrate the PCMs, fins and porous medium. Measurements of the PV operation temperatures and power output will be performed, and conversion efficiencies will be evaluated under laboratory conditions.

1.4 Thesis Organization

Present thesis is composed of six chapters, which are; introduction, literature review, methodology, experimental scheme, results & discussion and conclusion. Previous studies on solar energy along with TR of PVs are presented in chapter two. Chapter three describes the methodology followed for the realization of this thesis and the specifications of tools and materials which are used. Chapter four elaborates the manufacturing of the passive hybrid TR systems and the experimental procedure for measuring the associated parameters. Chapter five presents the results with discussion. Chapter six interprets the major findings, draws conclusion along with suggestions for further studies with recommended experimental designs.

Chapter 2

LITERATURE REVIEW

2.1 Overview

Maximization of energy harvesting and utilization of renewable energy sources are key points to make humankind, as well as the environment, free from fossil fuels. Specifically, if the point of interest is generation of electrical energy from solar energy, based on up-to-date PV technology, keeping PV cell temperatures as low as possible is not only having crucial role on energy harvesting, but also on thermal stresses on PV panels. This chapter presents brief history of solar energy harvesting through PVs and studies on passive TR of PVs by means of PCMs, porous medium and integrated PCMs and porous medium.

2.2 Historical Development of Photovoltaics

As the first step of photovoltaics, Becquerel invented photovoltaic effect as a result of his observation of electric current generated by a silver coated platinum electrode under light at late 19^{th} century [17,18]. In 1873, Smith found that the element Selenium is photoconductive and four years later, in 1877, Adams and Day revealed that the same element can generate small amount of electricity when it is exposed to light [19,20]. Fritts, manufacture the first ever PV panel from selenium wafers with gold plates in 1883 [21]. To create asymmetric electronic junctions, Schottky barrier devices needed for early PV cells –by thin layers of semi opaque metals on top of semiconductors– [22]. Hallwachs, in 1904, discovered that copper and cuprous oxide is photosensitive, that means those element and its compound can generate electric

current with the stimulation of light [23]. After a decade, Czochralski, paved a way for growing single silicon crystals by pulling wires composed of single crystalline of low melting points such as tin and zinc from melts [24].

Chapin, Fuller and Pearson, were the first manufacturers of PVs with silicon p-n junctions and according to their study that is conducted in 1954, a cell generated electricity with a rate of 60 watts per square meter of PV surface. That means researchers achieved to harvest approximately 6% of the solar radiation in order to produce electricity. In addition to that, researchers calculated the maximum reachable efficiency for entire solar spectrum is nearly 22% without any system loss [25]. At the same year, Kuwabara conducted experiments on cadmium sulphide and he discovered that the thin films of given compound is photoconductive [26]. Four years later, Vanguard 1 satellite was equipped with six single crystal silicon solar cells with 10% efficiency and area of 0.8 cm2. As a result of this space application, solar energy harvesting become more promising [27,28]. In another space application, in 1959, Explorer VI satellite was sent to the space with four paddles of PV –each containing 2,000 solar cells- [29].

As a result of energy crisis in 1970s, the world shifted to find other energy resources than fossil fuels. PVs were subjected a great interest and humankind tried its best to achieve higher energy conversion efficiencies with cheaper and commercially achievable PV technologies. Perlin, Berman and his research group –with economical help of Exxon Corporation- used low cost crystalline silicon wafers unlike space industry to manufacture semiconductors for PV cells and this was a major improvement commercialization of PVs. Moreover, polycrystalline and amorphous silicon along with organic conductors and thin films were added to the strategic

scheme to decrease PV cost [22,30]. Carlson and Wronski managed to fabricate the first PV cells from amorphous silicon [31].

In 1982, the first solar car, also known as the Quiet Achiever or BP Star Trek, was driven by Hans Tholstrup more than 4,000 km in 20 days with average speed of 30 km/h [32]. ARCO Solar, in 1983, built a 6-megawatt DC substation that is interconnected to the grid in California with two-axis trackers. Each tracker had 256 single crystal solar cell modules and the total area of the PV generators was approximately 80,937 m2 (20 acres) [33]. Green and his research group broke the efficiency barrier of 20% for silicon solar cells with one sun condition in 1986 with the efficiency of 20.6%, and they later on achieved higher efficiencies [34,35]. Researchers from University of South Florida built thin film PV cells with cadmium telluride and this invention was capable of converting 15.9% of the incident radiation into electric energy. This was the highest efficiency for thin films until 1992 [36]. Wilt et al. used PV cells containing gallium, indium and arsenide in their study in 1994, as a result of their study, given system efficiency could reach 30% with some alterations such as material optimization as well as anti-reflective coating [37].

PV cells are used also in aeronautical industry, aside from model R/C planes, manned flights were conducted with solar energy. Garton created an 80W solar powered under 2 kg (4 lb) model plane with a wingspan of nearly 5.5 m (18 ft) in 1993. Five years later, Beck made a flight with a similar plane –solar solitude- with the weight of 2 kg (4.4 lb) and wingspan of a little over 2.7 m (8.9 ft) using a 63 W of solar cells. University of Stuttgart built Icaré 2, used the information supplied by Beck's previous studies and solar aircraft –solar excel-, and this airplane was piloted by Klaus Ohlmann in 1996. Icaré 2 had wingspan of 25 m, weight of 270 kg, and its maximum and on-

hover powers were 14 and 1.8 kW respectively [38–40]. NASA, in 2002, built remotely controlled aircraft Pathfinder Plus with total of 12.5 kW solar array and this aircraft has wingspan and weight of 36.3 m (121 ft) and 315 kg (700 lb) respectively [41].

2.3 Phase Change Material-based Thermal Regulation of Photovoltaic Panels

Usage of PCM in TR of Si and Ge solar detectors on the Pioneer-Venus spacecraft paved a way for researchers to use PCMs in passive TR applications [42,43].

In 2010, experimental test was conducted to investigate the PCM performances on TR of PVs with five different PCMs, which were paraffin (RT20), eutectic (capric-lauric acid), eutectic (capric-palmitic acid), salt hydrate ($CaCl2{\cdot}6H2O$) and commercial blend (SP22). As a result of this study of, researchers found that the best option was salt hydrate and this compound created the highest cooling of 10°C temperature decrement in PV temperature after five hours of 1000 W/m2 solar irradiation [44]. Later, researchers performed another experimental work by comparing capric-palmitic acid with salt hydrate in outdoor environments in Dublin, Ireland and Vehari, Pakistan. As the results show, under around 330 W of incident solar energy on PVs with dimensions of 771 mm × 665 mm, salt hydrate –has about 7°C higher melting point- created a larger increment in electrical energy generation efficiency [45,46].

Along with experimental studies, effect of transition temperature of PCMs on electrical generation of PVs also studied numerically. Electrical performance of PV panels with PCMs having different melting points –melting areas of 9-10°C, 17-19°C, 22-26°C and 34-36°C- of organic paraffin compounds were compared with dynamic simulation

processes with central European weather conditions. As a result of this study, it is discovered that the optimum melting temperature for higher energy generation efficiency should be around 20°C [47]. According to another numerical study conducted with use of TRNSYS, with organic paraffin (RT28HC) used as a PCM, researchers found that maximum temperature difference with and without PCM can rise up to 35.6°C for a day, and it creates about 7% energy generation difference annually [48].

Although it is mentioned previously that 20°C melting point of PCM is optimal, weather conditions have a huge impact on TRs. An experimental study with organic paraffin PCM with melting rage between 38°C and 42°C were performed for hot climate zone –the United Arab Emirates-. Data acquisition was done on the average day of each month. Almost 6% yearly energy yield increment for PV-PCM system was shown at the end of this study [49]. In addition to this study, researchers logged temperature data of the same location throughout the year to investigate thermal behavior. Fatty acid ester (coconut oil) and petroleum jelly (Vaseline) have transition temperatures of 24°C and 44°C respectively. It is shown that petroleum jelly is a better option in contrast to fatty acid ester for intermediate and summer seasons whereas there is almost any difference between those PCMs for winter. Overall, when the mean operation temperatures are compared, PCMs used in that study showed 4°C temperature reduction, which refers about 2% energy generation increment [50].

Not only PCM specification and climatic conditions, but also heat conduction of PCMs and containers affects the TR of PVs. Researchers used expanded graphite composite to increase conductivity of PCM by adding the compound into the melted paraffin (ZDJN-28) with the mass ratio of 80% paraffin to 20% graphite composite. When it is

compared, the heat flow increased by 2 W/g with expanded graphite addition into PCM despite the latent heat of fusion of PCM is almost 40 kJ/kg higher than PCM/expanded graphite mixture. As a result of simulation and experimental work, system increased about 11.5% of maximum and 7.3% of average electric generation [51].

Researchers have also investigated approaches such as integrating additional heat transfer media to increase the heat flow to cool PVs down. A group of researchers used paraffin-based PCM (RT35) and Waksol of same density with metal fins to discover the convection and segregation. As a result of this study, they have observed that the heat transfer rate in PCMs increased due to increased surface area. On the other hand, presence of metal fins could lead bubble formations around the fins during the solidification of PCMs since PCMs shrink during this process [52]. Besides, Atkin and Farid came up with another experimental setup that has aluminum fin attached on the rear face of the PV along with aluminum fins are attached on the outer side of PCM container that has graphite-infused PCM inside and tested the rig numerically and experimentally. At the end of this study, researchers revealed that the overall efficiency, compared to the test case, which is untreated PV panel, only aluminum fins attached at the PV has the lowest efficiency increase. However, as the duration increases, effect of aluminum fins on the PCM container decreases [53]. A group of Turkish scientists focused on cooling techniques of PV panels experimentally. They used calcium chloride hexahydrate ($CaCl2{\cdot}6H2O$) as PCM and aluminum fins. After they had performed the experiment and compared the results of untreated PV, PV-PCM and PV-PCM with fins attached on the PCM tank, they have revealed that the minimum and maximum power differences are respectively around 0.36W and 2.84W

between the PV and PV-PCM and around 0.61W and 3.33W between PV and PV-PCM with fins systems [54].

Another fin-integrated PV-PCM study had been conducted in Iran under laboratory conditions. Researchers used 1 kW tungsten projectors to imitate sunlight and heat, polyethylene glycol 600 (PEG-600) and paraffin as PCMs and aluminum fins. As a result of the study, they discovered that paraffin-based systems –systems have higher melting point PCM- kept PVs cooler for longer periods of time [55].

Furthermore, researchers study on optimization of finned PV-PCM systems to increase the energy harvesting efficiency as much as possible. According to a numerical study carried on ANSYS Fluent 17.1, researchers showed that smaller spacing between fins needs more PCM mass since the melting process speeds up due to increased heat transfer surface. Additionally, it is showed that fin thickness should be around 2 mm to transfer the heat effectively as a result of conduction characteristics of metal bodies [56]. Bria et al. studied how the PCM thickness affects the performance of PV-PCM systems using paraffin (RT42) as PCM with fins numerically on ANSYS Fluent for Eastern Morocco according to the climate data collected from the meteorological station. Different PCM thickness values had been investigated during the study. As a conclusion, researchers showed that PCM with fins could be able to keep the system 32°C cooler than conventional PV panels and the optimal thickness for tested system is 6 cm, where the maximum output power is reached [57].

Not only infusions and fins but also porous media used along with PCMs for TRs of PVs. Duan numerically and experimentally studied a PCM with porous system to cool PVs. Researcher used metal foams with different porosities, coconut oil and paraffin-

based (RT42) PCMs and different inclination angles for examination. At the end of this study, it is found that the inclination angle and melting time are proportional and melting time at 90° inclination is 0.8 and 1.9 times longer than 0° inclinations for 0.85 and 0.95 porosities respectively. Additionally, it is showed that 0.90 porosity keeps solar cells the coolest at the end of 200 minutes of testing duration [58]. Another study that used copper foam as porous medium is directly attached on the rear panel of PV, paraffin wax as PCM and enclosure is closed with aluminum sheet. As a result, researchers showed that the PCM-copper metal foam provides better thermal performance than single PV and PV-PCM combinations. Electrical efficiency is about 10% for PV-PCM with copper foam, 9.85% for PV-PCM and 9.8% for bare PV [59]. Firoozzadeh and Shiravi used aluminum metal matrix as porous medium located at the back panel. The results revealed that electrical efficiency of PVs increased by 3.1% with PV-PCM with aluminum metal matrix and temperature reduction between PV with porous medium and PV-PCM with porous medium are 14.5°C and 18.8°C respectively. Researchers calculated that about 19% less solar cells are needed to build a 10 kW PV power plant [60]. For climatic affect testing, Sharaf et al. used aluminum metal foam as porous medium in aluminum reservoir that is filled with paraffin-based (RT44) as PCM during winter months. It is discovered that PV-PCM with aluminum metal foam decreased temperatures by 4.3%, 8% and 15%, that temperature differences increased the average power output by 1.85%, 3.38% and 4.14% for December, January and February respectively [61].

Chapter 3

MATERIALS AND EQUIPMENT

3.1 Introduction

It is desired to investigate the electrical generation and conversion efficiencies of PVs with and without passive hybrid TR systems through experimental and theoretical approaches. This chapter provides an overview of the materials and systems required for the experiments, as well as a detailed explanation of the manufacturing process of the systems.

3.2 Materials Used

In order to harvest solar energy, first and foremost, PV panels are needed. In order to provide cooling for PVs, reservoirs that incorporates PCMs with two different heat transfer elements –aluminum fins and aluminum porous medium– are considered. Four different cooling systems are manufactured. These are:

i- fins integrated with low melting point (25°C peak) PCM,

ii- porous medium integrated with low melting point (25°C peak) PCM,

iii- fins integrated with high melting point (35°C peak) PCM and

iv- porous medium integrated with high melting point (35°C peak) PCM.

In order to be visualized, PCM along with fin and porous configurations are given in Figure 3, Figure 4 and Figure 5.

Figure 3: Solid PCM [62].

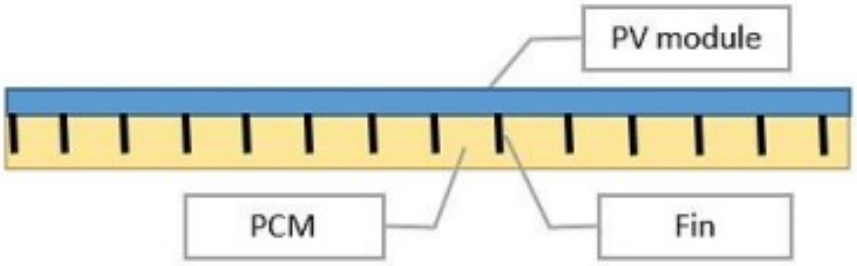

Figure 4: Schematics of fin integrated PV-PCM systems [63].

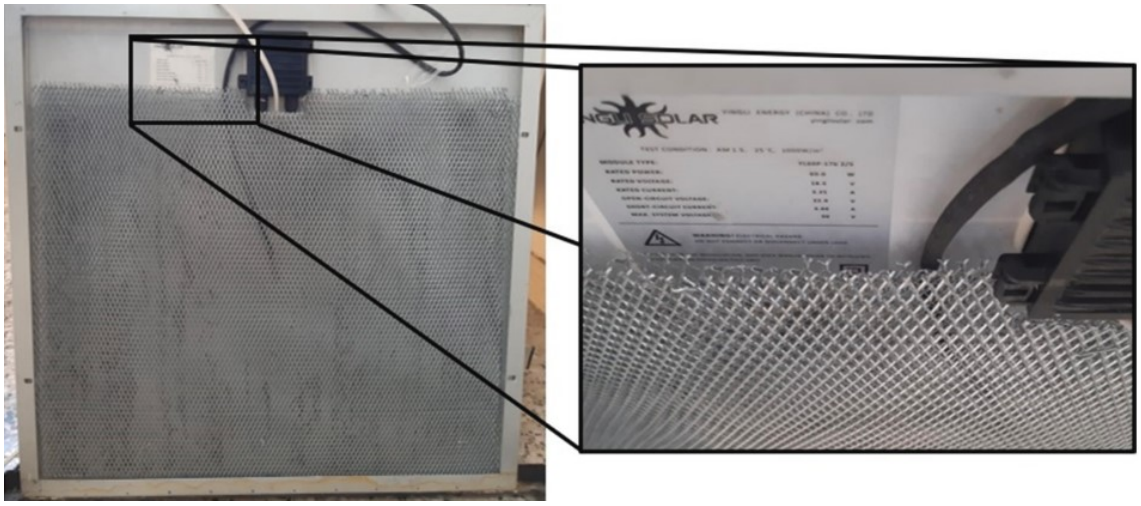

Figure 5: Porous medium integrated PV panel [64].

The PCMs and heat transfer elements will be accommodated in aluminum reservoirs that will be attached on back of the PV panels. Since the experiment will be performed

at laboratory conditions, two projectors (each has 500W halogen lamps) are used as the heat and light source.

3.2.1 Photovoltaic Panels

Three identical TommaTech TT55-36P PV panels having 55W of maximum power output are used in this study for different hybrid system configurations (one for the test case, one for the low melting point PCM configurations and one for the high melting point PCM configurations). Panel specifications are given in the Table 1. Operational temperature of this panel ranges from -40 to +85°C, whereas nominal operation cell temperature (NOCT) of this particular product is 45°C±2°C [65].

3.2.2 Phase Change Materials

In this study, two different paraffin-based organic PCMs, with peak melting points of 25°C and 35°C, are used as latent heat storage elements of the passive hybrid TR systems. Properties of PCMs are shown in Table 2 and Table 3.

3.2.3 Heat Transfer Elements

To manufacture the heat transfer elements (fins and porous medium) and the reservoirs, untreated 1050 aluminum sheet metal with thickness of 2 mm is used. All the relevant material properties of aluminum are given in Table 4.

Table 1: PV panel specifications [65].

Property	**Value**
Maximum Power (P_{max})	55 Wp
Maximum Power Voltage (V_{mp})	19.73 V
Maximum Power Current (I_{mp})	2.83 A
Open Circuit Voltage (V_{OC})	23.22 V
Short Circuit Current (I_{SC})	3.00 A
Number of Cells	36
Cell Dimensions	52.25×157 mm
Panel Dimensions	680×554×20 mm
Output Voltage	12 V
Temperature Coefficient (I_{SC})	0.06 %/°C
Temperature Coefficient (V_{OC})	-0.31 %/°C
Temperature Coefficient (P_{max})	-0.38 %/°C
Operation Temperature	-40 to +85°C
Nominal Operation Cell Temperature (NOCT)	45°C±2°C

Table 2: Properties of Rubitherm RT25HC organic PCM [66].

Property	**Value**
Melting Area	22-26°C (Main Peak: 25°C)
Congealing Area	26-22°C (Main Peak: 25°C)
Heat Storage Capacity ± 7.5%	230 kJ/kg
Specific Heat Capacity	2 kJ/kgK
Solid Density at 25°C	0.88 kg/l
Liquid Density at 40°C	0.77 kg/l
Heat Conductivity	0.2 W/mK
Volume Expansion	12.5 %

Table 3: Properties of Rubitherm RT35HC organic PCM [67].

Property	**Value**
Melting Area	34-36°C (Main Peak: 35°C)
Congealing Area	36-34°C (Main Peak: 35°C)
Heat Storage Capacity ± 7.5%	240 kJ/kg
Specific Heat Capacity	2 kJ/kgK
Solid Density at 25°C	0.88 kg/l
Liquid Density at 40°C	0.77 kg/l
Heat Conductivity	0.2 W/mK
Volume Expansion	12 %

Table 4: Physical and thermal properties of 1050 aluminum alloy [68].

Property	**Value**
Density	2.71 g/cm^3
Melting Point	650°C
Thermal Expansion	$24\times10^{+6}$ /K
Modulus of Elasticity	71 GPa
Thermal Conductivity	222 W/mK
Electrical Resistivity	0.0282×10^{-6} Ω

3.3 Manufacturing and Preparation of the PV Thermal Regulation Systems

Passive TR systems are produced by incorporating PCMs with heat transfer elements in aluminum reservoirs which has dimensions of 355×285×40 mm. The fins are made from 2 mm thick aluminum sheets and have dimensions of 250×30 mm. Porous medium on the other hand is composed from perforated aluminum sheets (2 mm thick) with dimensions of 345×280 mm.

3.3.1 Manufacturing of Reservoirs

The manufacturing process of the reservoirs involves cutting 2mm thick aluminum sheets into 455x405 mm pieces for quadrangular part which contains the heat transfer elements and PCMs and 375x325 mm pieces for the top covers. The sheets, excluding the cover, are bent 50 mm from each end to form the side walls. The sides are then bent 10mm further to create flanges for attaching the covers. The final result quadrangular reservoirs with attached covers.

3.3.2 Manufacturing of Fin System

For manufacturing of fins, 12 sheets of 2 mm thickness are cut to have dimensions of 250×50 mm. The sheets bent from 20 mm from one of the long edges and are screwed on base plate of two reservoirs with 50 mm distance between two fins. The reservoir with the fins are illustrated in Figure 6 and Figure 7.

Figure 6: Reservoir with fins.

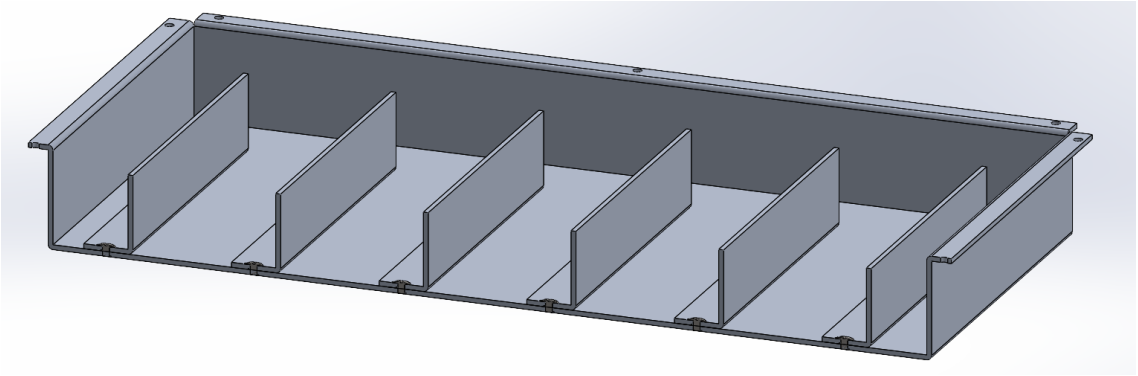

Figure 7: Cross-sectional view of reservoir with fins.

3.3.3 Manufacturing of Porous Medium

To manufacture porous medium, six sheets having 2 mm thickness are cut to have dimensions of 350×305 mm. After cutting process, those sheets are perforated by drilling with 12 mm diameter bit with center to center distance of 20 mm in staggered arrangement. The perforated sheets are on the side walls of two reservoirs. The reservoir with the porous medium is illustrated in Figure 8 and Figure 9.

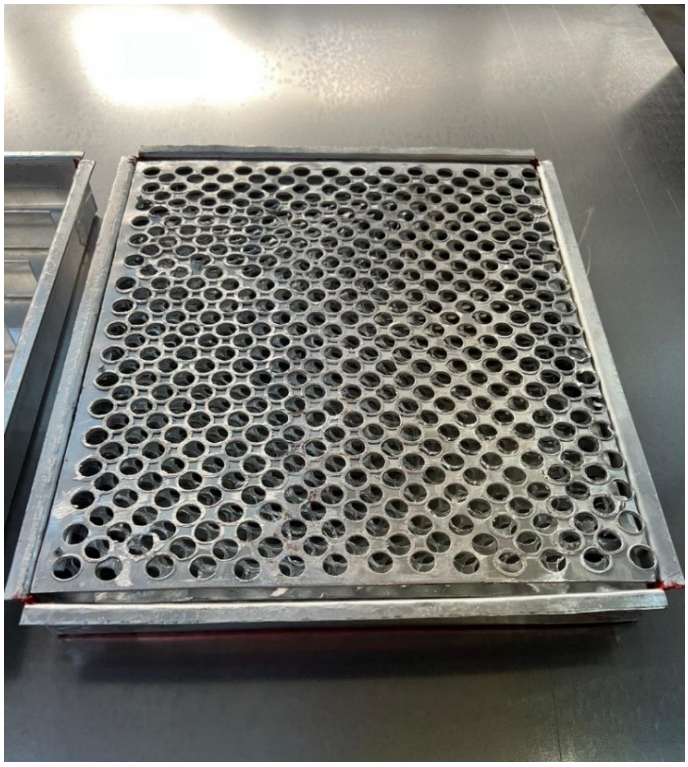

Figure 8: Porous medium as reservoir.

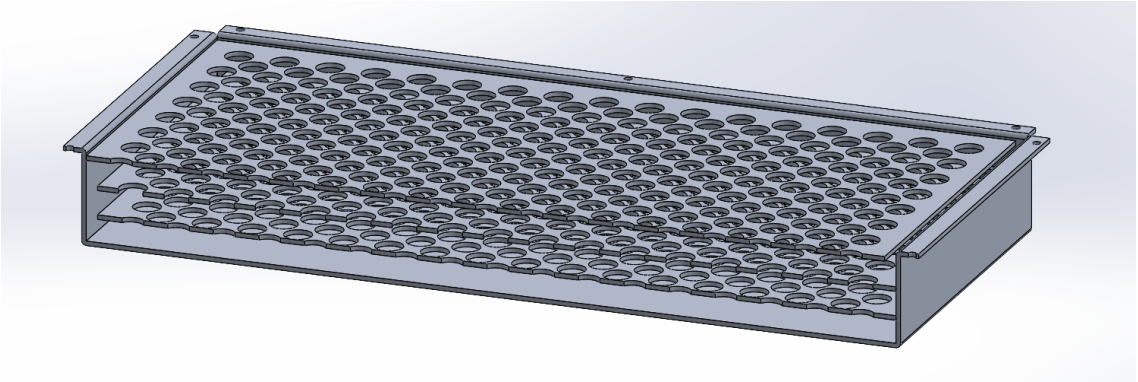

Figure 9: Cross-sectional view of porous medium as reservoir.

3.4 Preparation of Hybrid Systems

The first step in the manufacturing process of PCM-fin configuration involves screwing fins onto the base sheet of the reservoirs. PCMs are melted and poured in from the top. The flanges of the side walls are then sealed to prevent leakage, followed by attaching the cover sheets.

For the PCM-porous medium configuration, perforated sheets are attached to the side walls of reservoirs. The PCMs are then melted and filled into the reservoirs. The flanges of the side walls are then sealed as it is done for PCM-fin configuration, and the top covers are attached to complete the manufacturing process. Table 5 lists the different hybrid system configurations, while Figure 10 provides a visual representation of each stage of the manufacturing process.

Table 5: PCM melting point and heat transfer element configurations of cases.

	PCM Melting Point		**Heat Transfer Element**	
	25°C	35°C	Fin	Porous Medium
Case 1	×	×	×	×
Case 2	✓	×	✓	×
Case 3	✓	×	×	✓
Case 4	×	✓	✓	×
Case 5	×	✓	×	✓

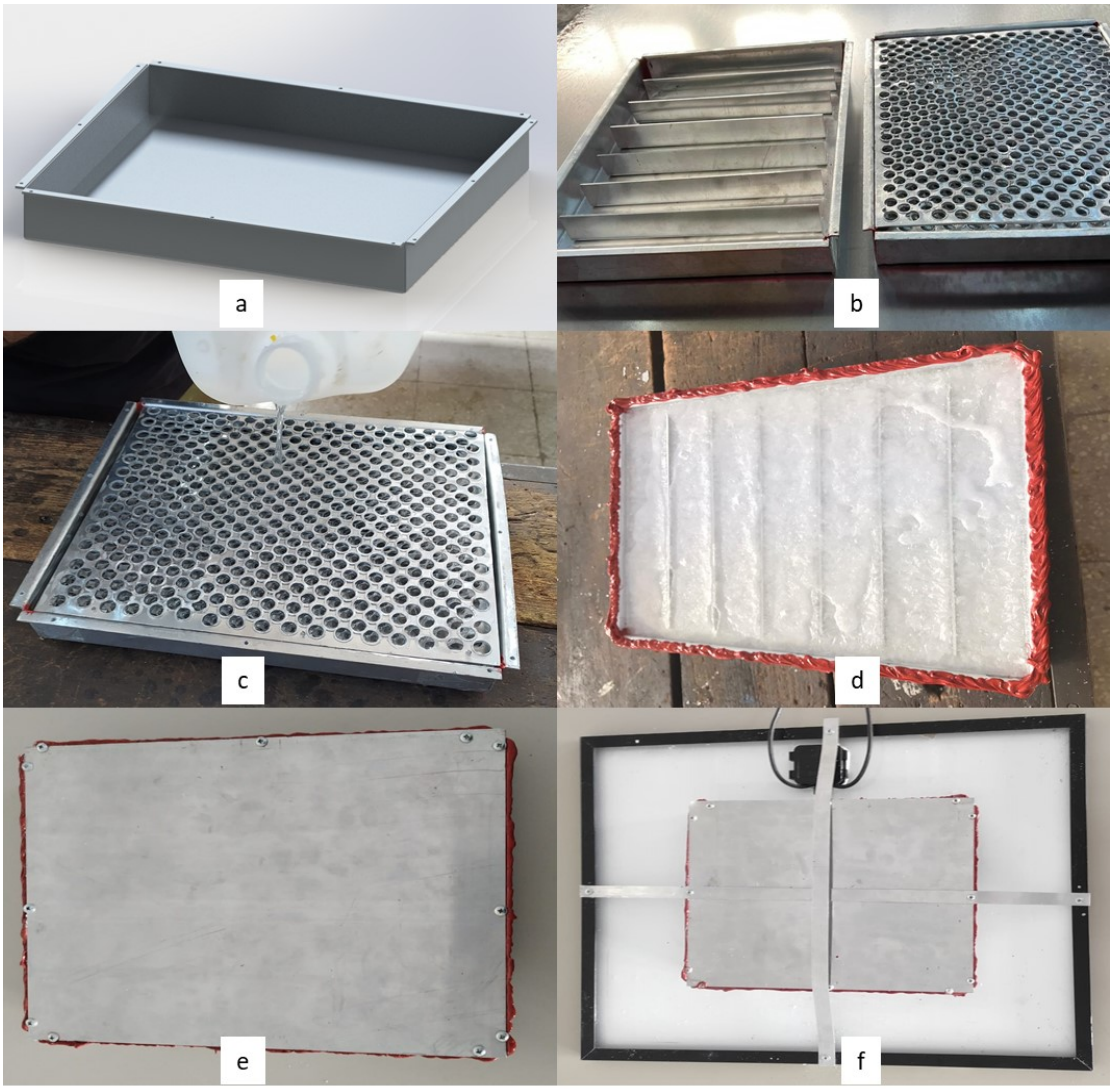

Figure 10: Manufacturing process of hybrid systems. (a) Reservoir, (b) reservoirs with fins and perforated sheets, (c) PCM addition, (d) hybrid system with solidified PCM, (e) fully assembled hybrid cooling system, (f) hybrid cooling system coupled with PV.

Chapter 4

EXPERIMENTAL PROCEDURE

4.1 Introduction

In this chapter, experimental steps are explained by elaborating the experimental setup as well as the process for data collection and analysis.

4.2 Experimental Setup

The experimental setup was created by manufacturing a steel stand with a 30° tilt angle. The heat and light source, consisting of two 500W halogen projectors, was attached to the steel arm, which was positioned parallel and 400 mm away from the PV panel. Three thermocouples were placed on top of the glass cover of the PVs, as shown in Figure 11. One of these thermocouples was positioned in the middle of the PV panel, while the other two were placed in the middle of the upper half of the PV and at the upper left corner of the rightmost solar cell of the bottom array. The ends of the thermocouples were connected to a data acquisition module. The manufactured hybrid systems were attached to the center of the rear face of the PVs by using aluminum strips. A DC motor was also connected as a load. The actual test rig and schematic of the experimental setup can be seen in Figure 12 and Figure 13, and detailed engineering drawings are included in Appendix C.

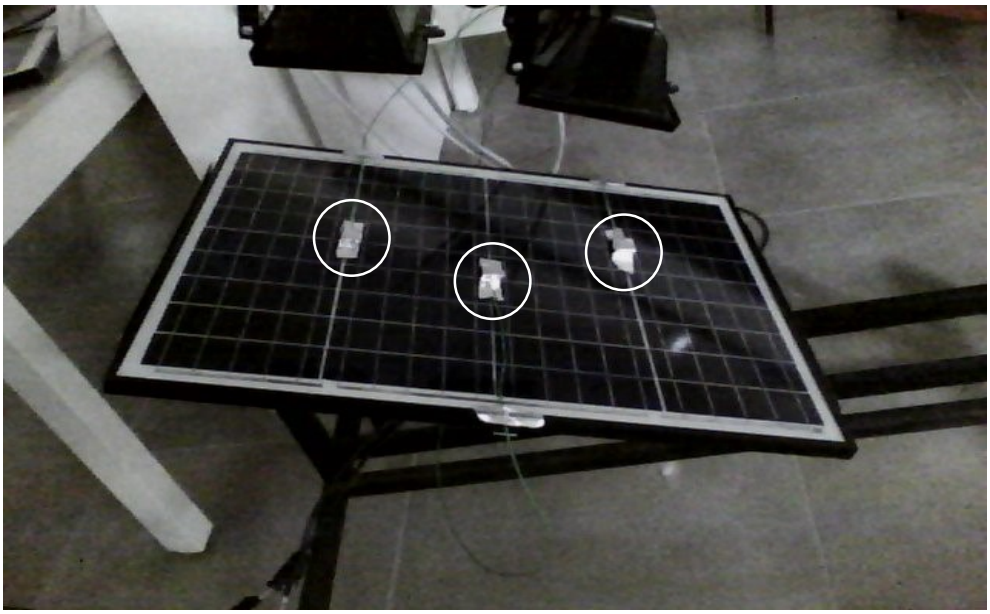

Figure 11: Thermocouple placements.

Figure 12: Test rig

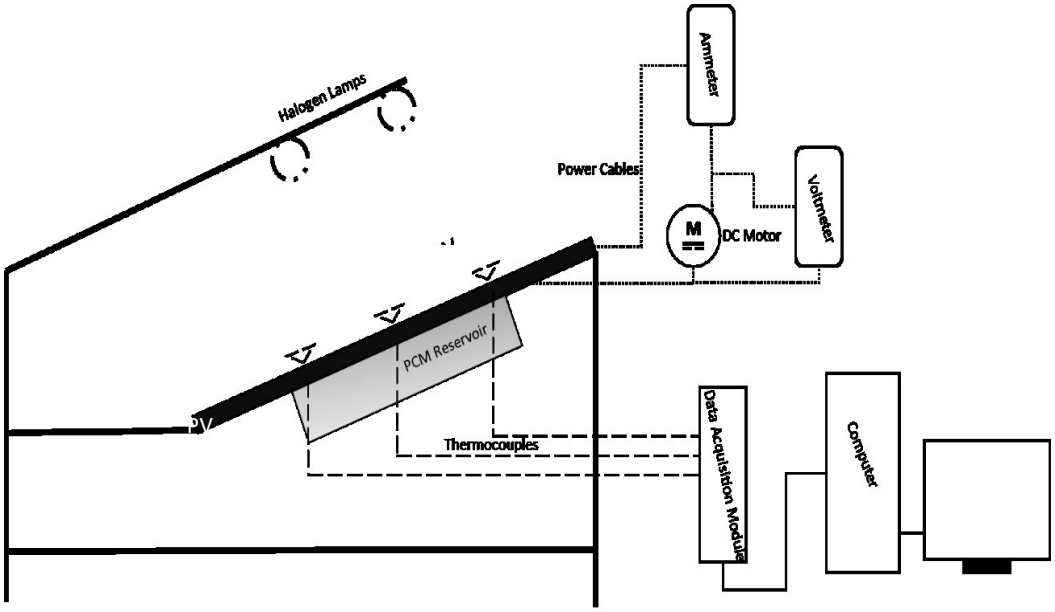

Figure 13: Schematics of test rig

4.3 Experimental Procedure

Before conducting the experiments, the EPLAB Precision Standard Pyranometer was connected to the MEGGER AVO M808 digital avometer, and it was determined that the irradiance of the light source was 950 W ± 1%. The PV or PV-PCM hybrid systems were then introduced to the experimental setup, and the DC motor was attached to the power cables of the PV. The thermocouples were placed on the glass cover, and the experiment began. The temperature readings of the PVs were logged every minute, while the experimental power output data was logged every fifteen minutes for 210 minutes. At the end of the experiment, the logged temperature data from the three thermocouples was collected to calculate the average temperature of the PVs for each minute.

4.4 Data Acquisition

For the data acquisition, K-type thermocouples made up from the NiCr-Ni wires are connected to Omega OMB-DAQ-3000 1-MHz, 16-Bit USB data acquisition module to collect temperature readings every minute for 210 minutes.

Experimental power output data is logged every fifteen minutes for 210 minutes with the help of AVO M808 avometer with 60W 24V DC motor load, and the theoretical output power is calculated according to the equations in the studies of Kant et al., and Evans and Florschuetz based on reference values of PV panel and the instantaneous temperature of the PVs [5,69]. The equations of efficiency, output power based on instantaneous temperature of solar cells and instantaneous output power of the PV panel are:

$$\eta_T = \eta_{ref}\left[1 - \beta_{ref}\left(T_{PV,t} - T_{ref}\right)\right] \quad (1)$$

$$P_{out,T} = \eta_T A_{cell} G \quad (2)$$

where η_T along with η_{ref}, β_{ref}, $T_{PV,t}$ and T_{ref} mean theoretical efficiency, reference efficiency, power decrement rate per unit temperature increment, instantaneous temperature and reference temperature of PV respectively.

$$P_{out,E} = V_t I_t \quad (3)$$

$$\eta_E = \frac{P_{out,E}}{G} \quad (4)$$

where $P_{out,T}$ means theoretical power output while A_{cell} and G are solar cell area and irradiation. $P_{out,E}$ stands for experimental power output, V_t and I_t mean instantaneous voltage and current which PV is generating respectively. Lastly, η_E is experimental efficiency.

4.5 Analysis of Results

In the analysis of results, thermally untreated PV (Case 1) will be compared to PV-fin system with low melting point PCM (Case 2), PV-porous medium system with low melting point PCM (Case 3), PV-fin system with high melting point PCM (Case 4)

and PV-porous medium with high melting point PCM (Case 5) based on two main criteria, which are PV cell temperature and efficiency of outlet power.

4.5.1 Photovoltaic Temperature Analysis

For the temperature analysis, three NiCr-Ni thermocouples are attached on front faces of PV panels –radiation exposed face- under 10 mm of insulation material and to reinforce the coupling of thermocouples, aluminum tape is used. In addition to thermocouples, thermal camera is also used to visualize the real-time temperature distribution on PVs. Thermal imaging of PVs is shown in Figure 14.

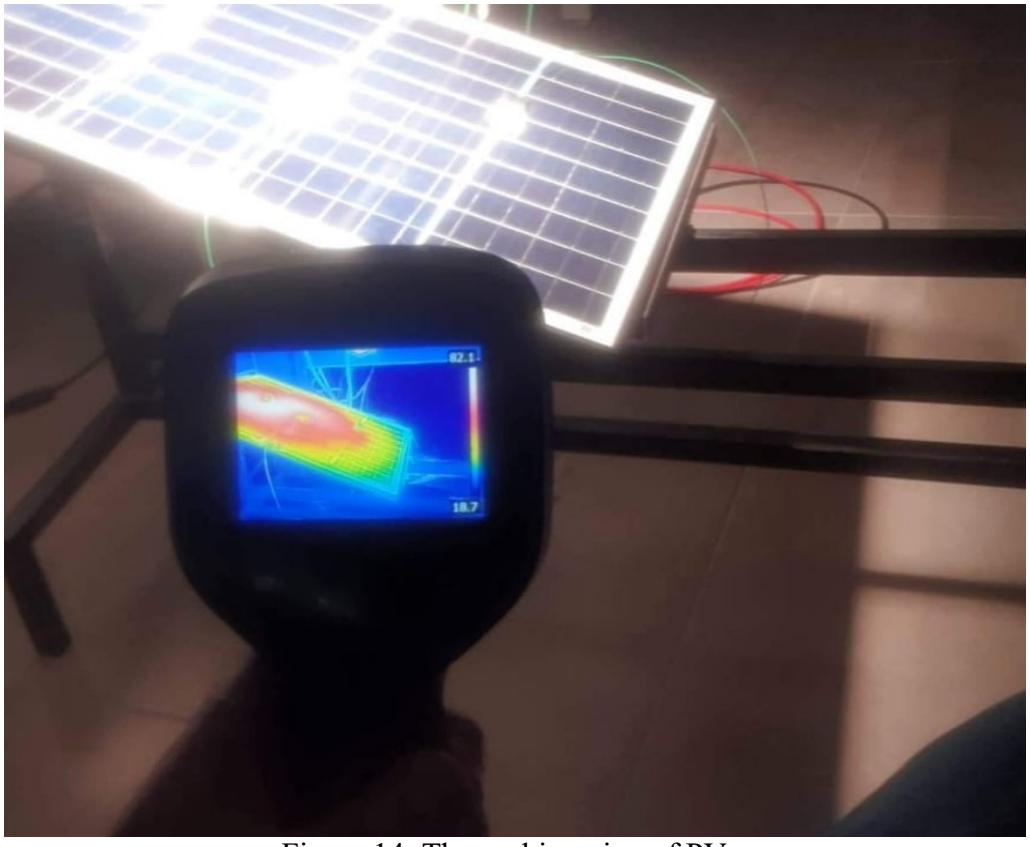

Figure 14: Thermal imaging of PVs.

4.5.2 Power Analysis

Equations 1 and 2 given above are employed to calculate the theoretical efficiency and theoretical power output analysis by using the catalogue information of the employed

PVs and the temperature data which is collected during the experiment. Numerical work is done with Microsoft Excel 2016. For the experimental power and efficiency analysis, voltage and current readings collected for every fifteen minutes throughout the experiment are multiplied to obtain instantaneous power output as it is given in Equation 3 then this power is divided by irradiation as it is shown in Equation 4 in order to obtain experimental efficiency values. The power generation curves are compared on the same chart as it is done for temperature analysis.

4.6 Error Analysis

The error analysis for the experiment was done based on uncertainty analysis calculation which is based on the equipment uncertainties provided by manufacturers. The formulas needed for the error analysis are [70]:

$$\frac{\delta_{\eta_E}}{\eta_E} = \sqrt{\left|\left(\frac{\delta_{EP}}{EP}\right)^2 + \left(\frac{\delta_G}{G}\right)^2\right|} \tag{5}$$

where $\frac{\delta_{\eta_E}}{\eta_E}$ inaccuracy of experimental efficiency whereas $\frac{\delta_{EP}}{EP}$ and $\frac{\delta_G}{G}$ are uncertainties of experimental power and irradiation. In order to measure uncertainties of experimental power and irradiation, we need Equation 6 and Equation 7. Which are:

$$\frac{\delta_{EP}}{EP} = \sqrt{\left(\frac{\delta_V}{V}\right)^2 + \left(\frac{\delta_I}{I}\right)^2} \tag{6}$$

$$\frac{\delta_G}{G} = \sqrt{\left(\frac{\delta_V}{V}\right)^2 + \left(\frac{\delta_P}{P}\right)^2} \tag{7}$$

where $\frac{\delta_V}{V}, \frac{\delta_I}{I}$ and $\frac{\delta_P}{P}$ are the uncertainties of voltage, current and pyranometer respectively.

For this study, theoretical analyses have also some uncertainties since theoretical calculations also need temperature and irradiance in order to be performed.

$$\frac{\delta_{\eta_T}}{\eta_T} = \frac{\delta_T}{T} \tag{8}$$

In Equation 8, $\frac{\delta_{\eta_T}}{\eta_T}$ means inaccuracy of theoretical efficiency, and $\frac{\delta_T}{T}$ stands for the uncertainty of temperature readings.

$$\frac{\delta_{TP}}{TP} = \left| \frac{2\delta_G}{G} - \sqrt{\left(\frac{\delta_G}{G}\right)^2 + \left(\frac{\delta_T}{T}\right)^2} \right| \tag{9}$$

Where $\frac{\delta_{TP}}{TP}$ means uncertainty of theoretical power.

$$\frac{\delta_T}{T} = \sqrt{\left(\frac{\delta_D}{D}\right)^2 + \left(\frac{\delta_{TC}}{TC}\right)^2} \tag{10}$$

In Equation 10, $\frac{\delta_D}{D}$ and $\frac{\delta_{TC}}{TC}$ mean uncertainties of data acquisition module and thermocouples respectively.

As a result of these equations, uncertainties of experimental efficiency, experimental power and irradiation are measured as 0.57%, 0.28% and 0.63%. Whereas, uncertainties of theoretical efficiency, theoretical power and temperature are found to be 0.85%, 0.16% and 0.85% respectively.

Chapter 5

RESULTS AND DISCUSSIONS

5.1 Introduction

In this chapter, results and discussion are presented. Effect of cooling systems on temperature, power output and efficiency of PVs are elaborated. Both experimental and theoretical results for power output are expressed and discussed.

5.2 Temperature of the Photovoltaic Panels

As the front panel temperatures are logged via three thermocouples, average of those temperatures are calculated and referred as the PV temperature of the respective cases. PV temperatures are illustrated in Figure 15.

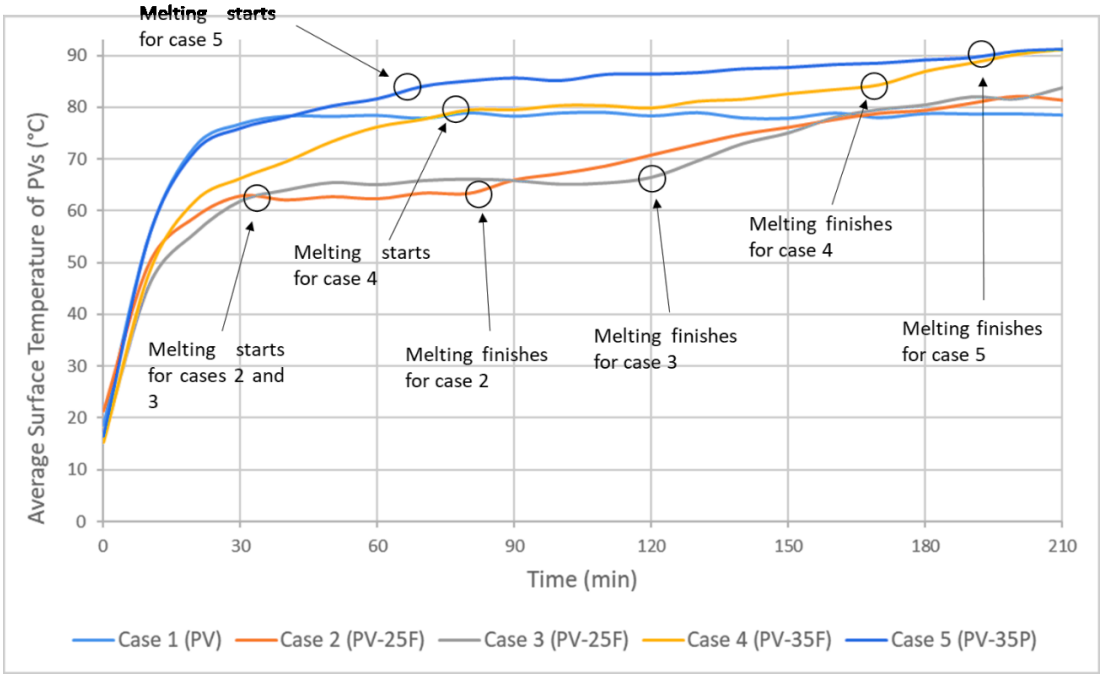

Figure 15: Temperature of PVs.

As shown in Figure 15, at a room temperature of 18°C, configuration of case 2 has the best cooling performance of all cases. However, with a slight temperature increase, case 3 keeps the PV cells cooler for a longer time. During the 210-minute experiment, it was found that configurations used in cases 2 and 3 cooled the PV cells on average by 7.2°C and 7.8°C, respectively. In terms of the instantaneous maximum temperature difference, low melting point PCM with fins cooled the PV by 17.6°C, while low melting point PCM with porous medium cooled it by 17°C. On the other hand, configurations employed in cases 4 and 5 actually increased the cell temperatures. During the experiment, the average increase in PV temperatures compared to the control case was 0.9°C for case 4 and 6.3°C for case 5.

Additionally, the heating curves of respective cases show that the melting process is faster for configurations with fins than for configurations with porous medium. This is because of the orientation of employed heat transfer elements. Fins are vertical and transfer heat to the PCMs at a faster rate, while the perforated sheets are horizontal and create a layer-by-layer melting of the PCMs in the porous medium. The cooling rates are higher for fin configurations, but the duration of high cooling is shorter. In contrast, the porous medium provides a longer cooling time.

Comparing the melting point of the PCMs, it is clear that configurations with a lower melting point cool down the PVs more effectively. However, it must be noted that the ambient temperature affects the melting trend of PCMs. With a high melting point PCM, the PVs must reach higher temperatures to supply enough energy to melt the PCM, as the PVs are the only heat source. The low melting point PCMs are therefore more appropriate for TR of PVs in colder climates. The presence of a high melting point PCM in cases 4 and 5 actually increases PV temperatures due to its heat storage

characteristics and the reduction in heat transfer area between the PV and the environment.

Figure 16 illustrates the thermographic images of the PV panels at the minute of 210. It can be seen that the PV without any cooling system has a more uniform distribution of hot areas compared to those with cooling systems. The PV panels with cooling systems have concentrated hot regions, leading to less uniform heat dissipation. The presence of a PCM reservoir concentrates the hot area on the PV because of its higher heat transfer rate from the PV to the reservoir than the PV to the surrounding air. The thermal camera photographs also show that the lower melting point PCMs (cases 2 and 3) have lower temperatures at the thermal concentration area than the PCMs with a higher melting point (cases 4 and 5). Choosing PCMs with higher melting points in colder climates is therefore more likely to cause mechanical damage to the PVs due to thermal stress.

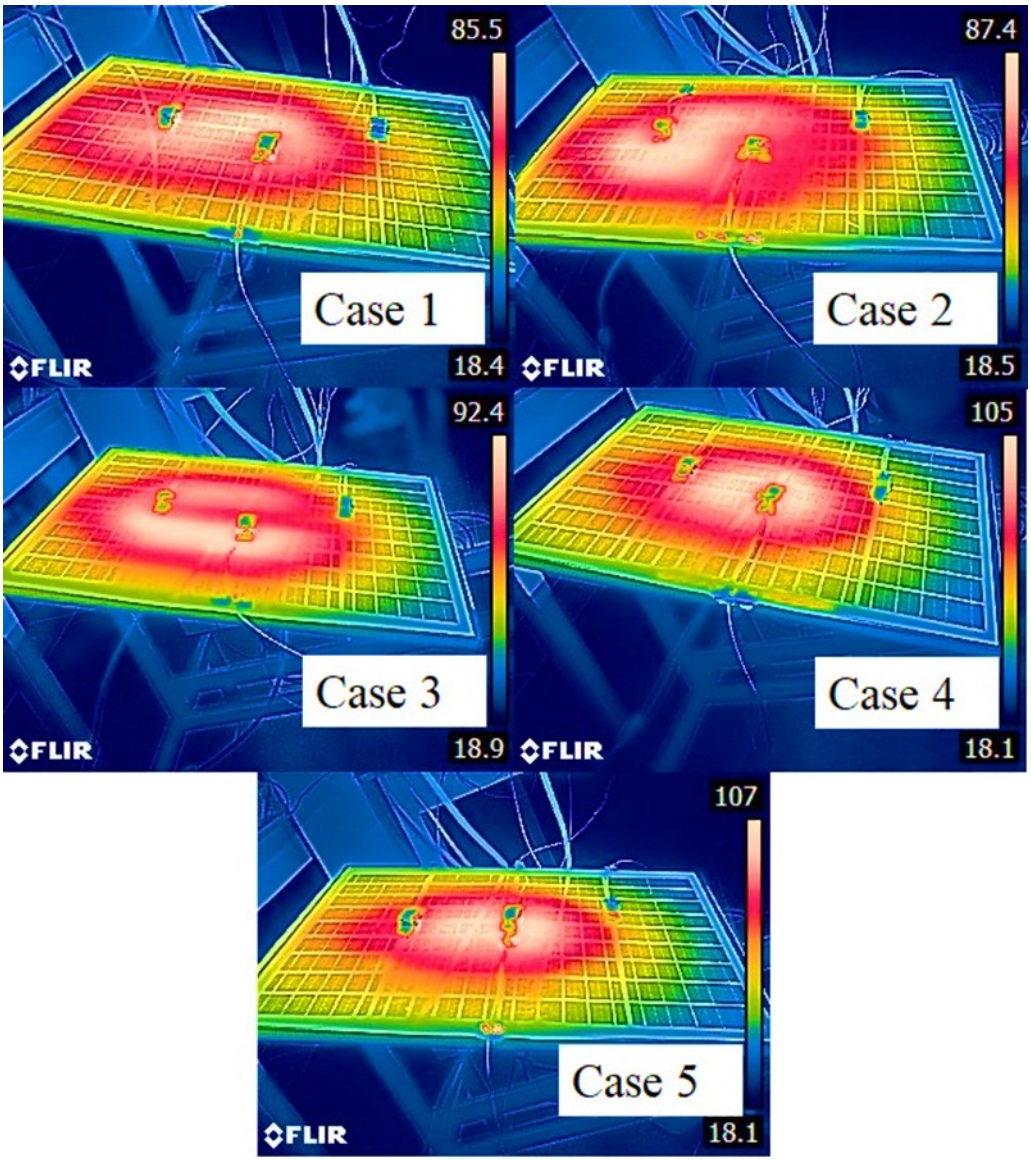

Figure 16: Thermal camera photographs taken at the end of the experiments for all cases.

5.3 Power Generation and Efficiency

There are two power output and efficiency results for the respective cases as described in section 4.3: i- experimental and ii- theoretical. The experimental power output results are given in Figure 17, whereas theoretical results are given in Figure 18.

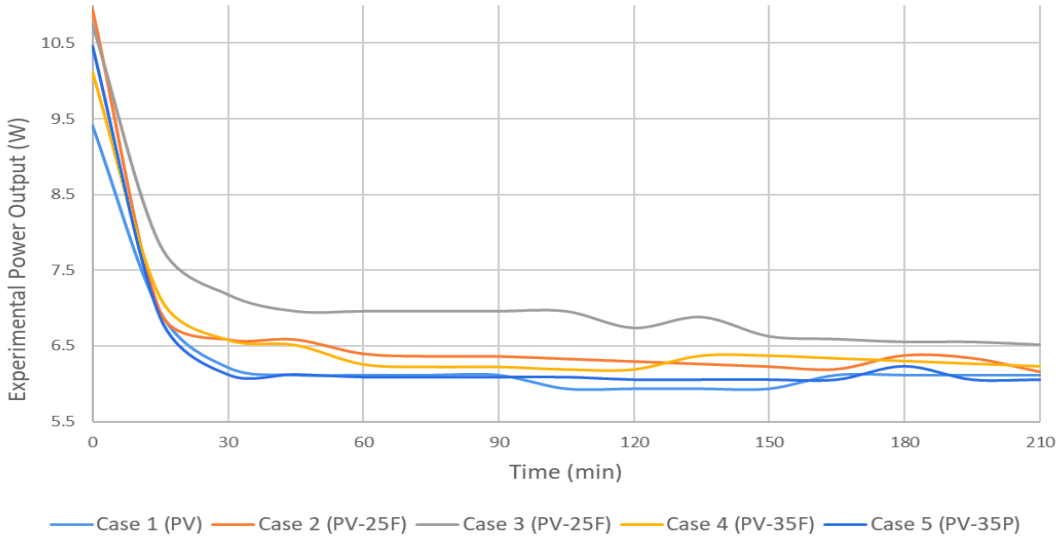

Figure 17: Experimental power output of PVs during tests.

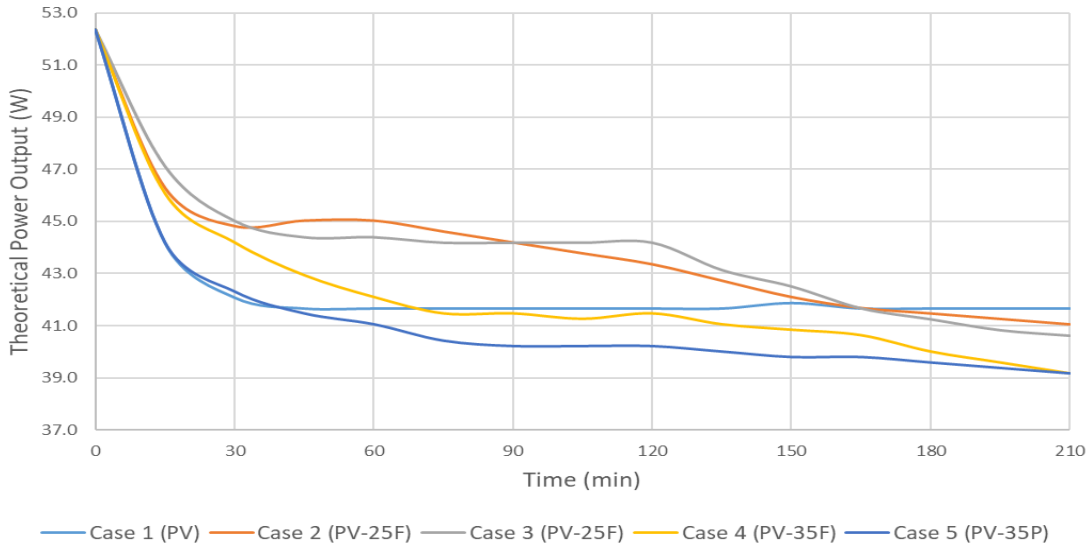

Figure 18: Theoretical power output of PVs during tests.

It is clear from Figure 17 and Figure 18 that the general trends of the power degradation as time proceeds (PV temperature increases) are similar for experimental and theoretical cases, though the power generation rates differ significantly. The main cause of the difference in the power generation rates of the theoretical and experimental cases is the source of light. Equation 1 and Equation 2 give the theoretical efficiency and the power generation rate of PVs under solar irradiation; however, the

experiments were conducted under laboratory conditions with two halogen projector light sources with total power of 1000 W. Although the artificial light source enabled PVs to generate power to run the DC motor, the generated currents were much lower than those that are generated with sunlight.

Figure 17 also shows that, experimental power generation of the case 3 is the highest throughout the experiment. Although Cases 4 and 2 both have higher power outputs than Cases 1 and 5, Case 2 is the better option because it has a slightly larger area under the power generation curve. Not only case 1 but also case 5 have the worst power generation among all five experimental cases and if the power generation is the only concern, case 5 should be chosen over case 1 since the power generation curve is more consistent and energy generation is slightly higher. Yet, untreated PV is more financially feasible than configuration including PCM and aluminum reservoirs as well as aluminum porous medium.

When the theoretical power generation is the concern, it is obvious that Figure 15 and Figure 18 are mirror images of each other along x-axis since the used equation is providing a linear, inversely proportional relation between power generation and PV cell temperature. Based on Figure 18, it can be concluded that configurations with PCM with lower melting point is more suitable for energy harvesting in colder environments. Moreover, the untreated PV is also a better choice over configurations with PCM having higher melting points for feasibility in cold environments. In contrast to cold climates, PCMs having higher melting points should be used for warmer climates as the slopes of cases 2 and 3 are steeper than those of cases 4 and 5.

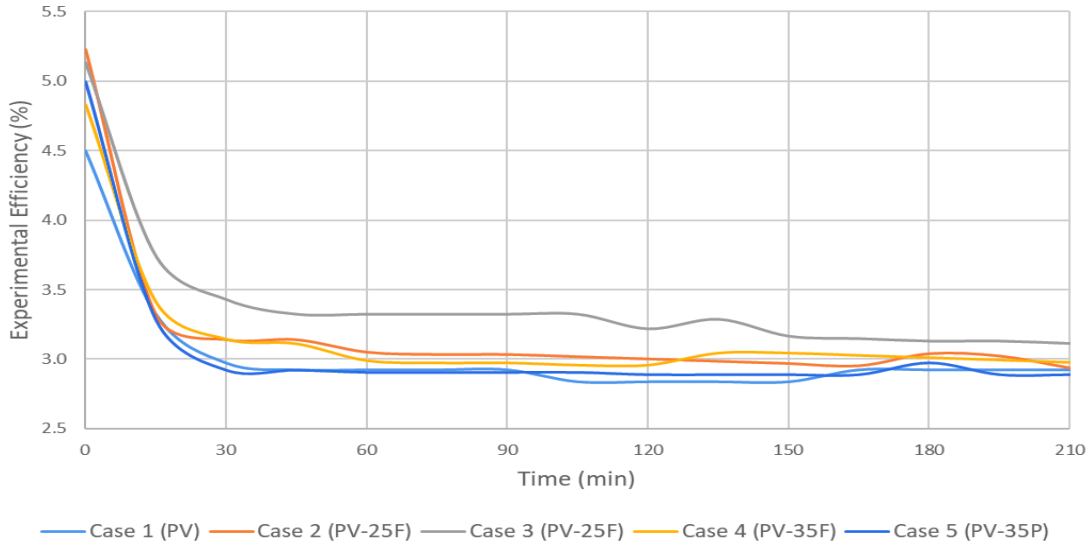

Figure 19: Experimental efficiencies during experiments.

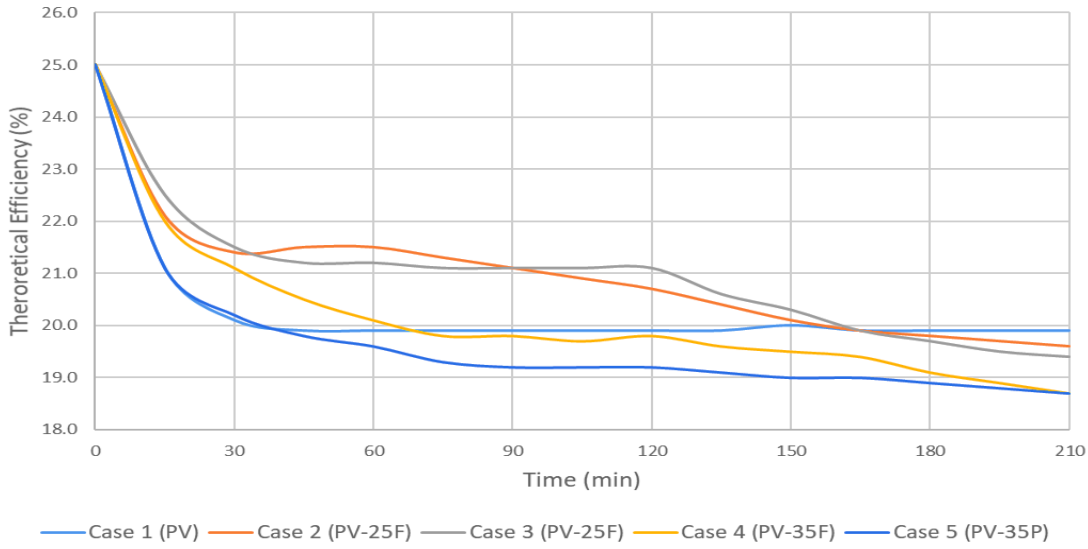

Figure 20: Theoretical efficiencies during experiments.

Figure 19 shows the experimental efficiencies which are calculated by the evaluated experimental power (by using Equation 3) and the measured irradiation (950 W/m^2) by pyranometer. Figure 20 on the other hand shows the theoretical efficiencies which are calculated by Equation 1 using measured PV temperatures. It is clear that Figure 19 is equivalent to Figure 17 and Figure 20 is identical to Figure 18 except the values

in the ordinate axis. This is expected since the definition of the efficiency is the generated power that is divided by the constant of irradiation on the panel area.

Table 6 shows the experimental efficiency enhancement of cases with respect to the test case whereas Table 7 lists the theoretical efficiency enhancement of cases respect to the test case throughout the experiments.

Table 6: Experimental efficiency increments with respect to the test case.

Time (min)	**Case 2 (%)**	**Case 3 (%)**	**Case 4 (%)**	**Case 5 (%)**
0	16.3	14.2	7.5	11.1
15	-0.1	12.6	2.7	-1.2
30	5.8	15.3	5.8	-1.6
45	7.5	13.6	6.4	0
60	4.4	13.6	2.2	-0.6
75	3.9	13.6	1.7	-0.6
90	3.9	13.6	1.7	-0.6
105	6.5	17.1	4.2	2.5
120	5.9	13.4	4.2	1.9
135	5.3	15.8	7.2	1.9
150	4.7	11.5	7.2	1.9
165	1.1	7.6	3.5	-1.1
180	4.1	7.0	2.9	1.8
195	3.5	7.0	2.4	-1.1
210	0.6	6.4	1.8	-1.1
Average	4.9	12.2	4.1	0.9

It can be seen in the Table 6 that case 2 performed as second-best in terms of efficiency enhancement. Using this hybrid system increases the efficiency by as much as 16% in the early stages of the heating process. However, this efficiency increment compared to the test case falls below 7% after an hour.

Case 3 is the best case for efficiency enhancement with PCM-based hybrid systems for TR. Over a long period of time, the efficiency increment is in double digits, means there is a significant amount of power generation which would be lost if there was no TR system.

Case 4 shows a single digit increase in efficiency throughout the experiment, it means this hybrid system can also be used even though the increase in power generation may not be significant.

Case 5 is not an effective hybrid system for enhancing efficiency or power generation in this study for PVs. Additionally, as the table shows, there is no stability in efficiency enhancement.

Table 7: Theoretical efficiency increments with respect to the test case.

Time (min)	**Case 2 (%)**	**Case 3 (%)**	**Case 4 (%)**	**Case 5 (%)**
0	0	0	0	0
15	4.7	6.6	4.3	0
30	6.5	7	5	0.5
45	8	6.5	3	-0.5
60	8	6.5	1	-1.5
75	7	6	-0.5	-3
90	6	6	-0.5	-3.5
105	5	6	-1	-3.5
120	4	6	-0.5	-3.5
135	2.5	3.5	-1.5	-4
150	0.5	1.5	-2.5	-5
165	0	0	-2.5	-4.5
180	-0.5	-1	-4	-5
195	-1	-2	-5	-5.5
210	-1.5	-2.5	-6	-6
Average	3.3	3.3	-0.7	-3

It is shown that case 2 has the highest increase in instantaneous efficiency gain of 8% which lasts for a short time interval. On the other hand, case 3 increases the instantaneous efficiency by 7% at maximum and this gain decreases only by 1% for 90 minutes. Cases 4 and 5, however, decrease the theoretical efficiency values instead of increasing as they increased the temperatures instead of decreasing.

As Table 6 shows the results of the real world study, average efficiency enhancements for cases with respect to the test case is more than the maximum efficiency enhancements for the theoretical cases given in Table 7. This difference may be due to the use of an artificial light source in the laboratory, which generates power that is about 20% of the theoretical case. This means 1 W difference in experimental case can increase the efficiency by 10% whereas this difference causes only about 1.8% enhancement for the theoretical case. On the other hand, for theoretical power calculation, which is given with Equation 2 is the formulized value with respect to the solar irradiation, instantaneous efficiency of the PV panel which relies on the instantaneous temperature of the solar cells and the solar cell area. Additionally, it has to be pointed out that although the coolest temperature of PVs is achieved with case 2, maximum experimental power generation, as well as the efficiency, is achieved by case 3. Differences in the microstructure of the polycrystalline PV panels used may also play a role in the difference in maximum power generation and efficiency between case 2 and case 3.

To further advance the applicability of this study, a feasibility analysis was conducted based on the given experimental power generation and efficiency enhancement figures and tables. The saving-to-investment approach was used with a 9% interest rate. It was determined that case 3 was the best option, with a return-of-investment time of 13

years. However, when considering the average efficiency enhancement values, case 2 would take over 100 years to recover the investment. The decrease in the life of the PV according to the thermal stress was not taken into account in this feasibility analysis. Further research should be conducted to investigate the effect of thermal stress on the service life of PVs for a more precise feasibility analysis. To summarize, case 3 is the only hybrid TR system that saves money and energy at the same time while generating electricity without combustion of harmful compounds is priceless.

Chapter 6

CONCLUSION

6.1 Summary of the Results

In this study, four different hybrid cooling systems having PCMs with two different melting points and heat transfer elements are tested with PV panels having maximum output power Rating of 55W. The tests are performed under laboratory conditions with average room temperature of 18°C and 950W/m^2 irradiation. At the end of the tests it has been found that:

- The highest instantaneous temperature drop with respect to test case is achieved by case 2 with 17.6°C.
- The lowest average temperature throughout the experiment is achieved by case 2 with 67.74°C.
- Porous medium elongated the melting duration of PCMs more than 40% compared to fins.
- Configurations used in cases 2 and 3 are increasing the theoretical efficiencies as much as 8% and 7% respectively, whereas in the reality, these increments are 16.3% for case 2 and 17.1% for case 3.
- Using low melting point PCMs for colder climates is more useful for TR and, the efficiency improvement.
- It can be said that the theoretical and experimental power output behaviors are verifying each other even though the curves do not fully overlap each other.

6.2 Conclusion

All over the world, since the fossil fuel reserves are getting closer to be consumed out each and every moment and carbon gases are exhausted as an end product of fossil fuel combustions which is end up with climate crisis, energy generation industry is forced to shift to harvest renewable energy sources such as wind, wave and sun. Although humankind discovered to use light as source for electric generation since 17th century, solar cells had to be improved a long way to convert promising rate of power and be financially available for majority of the world population. These days, as a result of the decrease in PV prices, electricity generation from solar cells surpasses 800 TWh. Yet, two centuries later, PVs are still fragile against high temperatures.

Due to the effect of irradiation, average temperature of PVs increases with time until the thermal equilibrium is achieved. In order to harvest the maximum energy possible from the sun, average temperature of the PV has to be regulated via cooling techniques since the temperature and efficiency of PVs are inversely proportional. This novel study offers PCM-based passive cooling techniques with two different paraffin-based PCMs with two different heat transfer elements which are fins and porous medium containing perforated sheets manufactured from 1050 aluminum alloy. When compared, the system that contains PCM with melting point of 25°C and fins has the maximum cooling capacity among all hybrid passive cooling systems although the system with low melting point PCM (25°C) with porous medium results with maximum efficiency one at the end of 210 minutes of experiment. On the other hand, hybrid systems which contain high melting point PCM (35°C) are not useful for the experimental conditions since the melting point is about 20°C above the environmental

temperature and the area that is occupied by the PCM reservoirs are lowering the heat transfer surface of the panels.

6.3 Future Work

To carry this study one step –or several steps- ahead, it is recommended to redo the same exact experimental procedures with same test rig during summer for the pure comparison of environmental effects and how those hybrid systems are performing for hot climates. In addition, with the use of fans, effect of the convection on heating curve of the PVs as well as the melting behavior of the PCMs can be discovered. Another suggestion is to do these experiments under direct sunlight with low environmental temperature and high environmental temperature with similar solar irradiances to show the difference in PV temperatures based on the PCMs which are used under different climatic conditions and to verify with the theoretical data which will be obtained with instantaneous temperatures.

REFERENCES

[1] Zhang Q, Agbossou A, Feng Z, Cosnier M. Solar micro-energy harvesting based on thermoelectric and latent heat effects. Part II: Experimental analysis. Sensors and Actuators, A: Physical 2010;163:277–83. https://doi.org/10.1016/j.sna.2010.06.026.

[2] International Energy Agency. Renewable electricity generation by technology, 1990-2026. 2021.

[3] Polman A, Knight M, Garnett EC, Ehrler B, Sinke WC. Photovoltaic materials: Present efficiencies and future challenges. Science 2016;352. https://doi.org/10.1126/science.aad4424.

[4] Our World in Data. Solar PV Module Prices n.d. https://ourworldindata.org/grapher/solar-pv-prices?time=2000..latest.

[5] Kant K, Shukla A, Sharma A, Biwole PH. Thermal response of poly-crystalline silicon photovoltaic panels: Numerical simulation and experimental study. Solar Energy 2016;134:147–55. https://doi.org/10.1016/j.solener.2016.05.002.

[6] Ma T, Yang H, Zhang Y, Lu L, Wang X. Using phase change materials in photovoltaic systems for thermal regulation and electrical efficiency improvement: A review and outlook. Renewable and Sustainable Energy Reviews 2015;43:1273–84. https://doi.org/10.1016/j.rser.2014.12.003.

[7] LG Energy. At what temperatures do the solar panels perform at their best? n.d. www.lgenergy.com.au/faq/solar-power-explained/at-what-temperatures-do-the-solar-panels-perform-at-their-best (accessed December 1, 2021).

[8] Boston Solar. How do temperature and shade affect solar panel efficiency? 2019. https://www.bostonsolar.us/solar-blog-resource-center/blog/how-do-temperature-and-shade-affect-solar-panel-efficiency/ (accessed December 1, 2021).

[9] Mazer JA. Solar cells. An introduction to crystalline photovoltaic technology. 1st ed. 1997.

[10] Hu J, Chen W, Qiu Z, Zhao B, Zhou J, Qu Y. Thermal performances of ETFE cushion roof integrated amorphous silicon photovoltaic. Energy Conversion and Management 2015;106:1201–11. https://doi.org/10.1016/j.enconman.2015.10.008.

[11] Makki A, Omer S, Sabir H. Advancements in hybrid photovoltaic systems for enhanced solar cells performance. Renewable and Sustainable Energy Reviews 2015;41:658–84. https://doi.org/10.1016/j.rser.2014.08.069.

[12] Skoplaki E, Palyvos JA. On the temperature dependence of photovoltaic module electrical performance: A review of efficiency/power correlations. Solar Energy 2009;83:614–24. https://doi.org/10.1016/j.solener.2008.10.008.

[13] Virtuani A, Pavanello D, Friesen G. Overview of Temperature Coefficients of

Different Thin Film Photovoltaic Technologies. 25th European Photovoltaic Solar Energy Conference and Exhibition/5th World Conference on Photovoltaic Energy Conversation 2010. https://doi.org/10.4229/25thEUPVSEC2010-4AV.3.83.

[14] Hasanuzzaman M, Malek ABMA, Islam MM, Pandey AK, Rahim NA. Global advancement of cooling technologies for PV systems: A review. Solar Energy 2016;137:25–45. https://doi.org/10.1016/j.solener.2016.07.010.

[15] Chandrasekar M, Rajkumar S, Valavan D. A review on the thermal regulation techniques for non integrated flat PV modules mounted on building top. Energy and Buildings 2015;86:692–7. https://doi.org/10.1016/j.enbuild.2014.10.071.

[16] Kant K, Shukla A, Sharma A, Biwole PH. Heat transfer studies of photovoltaic panel coupled with phase change material. Solar Energy 2016;140:151–61. https://doi.org/10.1016/j.solener.2016.11.006.

[17] Becquerel E. Studies of the effect of actinic radiation of sunlight by means of electric currents. Comptes Rendu Hebdomadaires de Séances de l'Académie Des Sciences 1839:561–7.

[18] Williams R. Becquerel photovoltaic effect in binary compounds. The Journal of Chemical Physics 1960;32:1505–14. https://doi.org/10.1063/1.1730950.

[19] Smith W. Effect of light on selenium during the passage of an electric current. Nature 1873:303.

[20] Adams WG, Day RE. The action of light on selenium. Philosophical Transactions of the Royal Society of London 1877;167:313–49. https://doi.org/10.1098/rstl.1877.0009.

[21] Fritts CE. On a new form of selenium cell and, and some electrical discoveries made by its use. American Journal of Science 1883;26:465.

[22] Nelson J. The Pysics of Solar Cells. London: Imperial College Press; 2003.

[23] Hallwachs W. Über die Strahlung des Lichtbogens. Annalen Der Physik 1904;318:38–64. https://doi.org/10.1002/andp.18943180103.

[24] Czochralski J. A new method for the measurement of crystallization rate of metals. Zeitschrift Für Physikalische Chemie 1918;92U:219–21. https://doi.org/10.1515/zpch-1918-9212.

[25] Chapin DM, Fuller CS, Pearson GL. A New Silicon p-n Junction Photocell for Converting Solar Radiation into Electrical Power. Journal of Applied Physics 1954;25:676–7. https://doi.org/10.1063/1.1721711.

[26] Kuwabara G. The Optical and Electrical Properties of Cadmium Sulphide Films. Journal of the Physical Society of Japan 1954;9:97–102. https://doi.org/10.1143/JPSJ.9.97.

[27] NASA. Vanguard 1. NASA Space Science Data Coordinated Archive 1958. https://nssdc.gsfc.nasa.gov/nmc/spacecraft/display.action?id=1958-002B.

[28] Easton RL, Votaw MJ. Vanguard I IGY Satellite (1958 Beta). Review of Scientific Instruments 1959;30:70–5. https://doi.org/10.1063/1.1716492.

[29] Newel HE. Scientific Findings From Explorer VI. Paper Knowledge Toward a Media History of Documents 1965.

[30] Perlin J. From Space to Earth: The Story of Solar Electricity. Harvard University Press, 2002, p. 54.

[31] Carlson DE, Wronski CR. Amorphous silicon solar cell. Applied Physics Letters 1976;28:671–3. https://doi.org/10.1063/1.88617.

[32] National Museum of Australia. The Quiet Achiever solar car n.d. https://www.nma.gov.au/explore/collection/highlights/quiet-achiever-solar-car.

[33] Tolbert REL, Arnett JC. Design, installation and performance of ARCO solar photovoltaic power plants. Conference: 17. IEEE photovoltaic specialists conference, 1984.

[34] Green MA. Recent Advances in Silicon Solar Cell Performance. Tenth E.C. Photovoltaic Solar Energy Conference, Dordrecht: Springer Netherlands; 1991, p. 250–3. https://doi.org/10.1007/978-94-011-3622-8_63.

[35] Green M, Zhao J, Wang A, Blakers A. One-sun silicon solar cell research 1993.

[36] Zweilbel (Editor) K. Polycrystalline Thin Films. 1993.

[37] Wilt DM, Fatemi NS, Hoffman RW, Jenkins PP, Brinker DJ, Scheiman D, et al. High efficiency indium gallium arsenide photovoltaic devices for thermophotovoltaic power systems. Applied Physics Letters 1994;64:2415–7. https://doi.org/10.1063/1.111585.

[38] North A. History of solar flight. Autonomous Systems Lab, Swiss Federal Institute of Technology 2008.

[39] Roberts C, Vaughan M, Bowman W. Development of a solar powered micro air vehicle. 40th AIAA Aerospace Sciences Meeting & Exhibit, Reston, Virigina: American Institute of Aeronautics and Astronautics; 2002. https://doi.org/10.2514/6.2002-703.

[40] Voit-Nitschmann R. Solar- und Elektroflugzeuge - Geschichte und Zukunft. Wechselwirkungen, Jahrbuch Aus Lehre Und Forschung Der Universität Stuttgart 2001. https://doi.org/10.18419/opus-3664.

[41] Gibbs (Editor) Y. NASA Armstrong Fact Sheet: Pathfinder Solar-Powered Aircraft 2017. https://www.nasa.gov/centers/armstrong/news/FactSheets/FS-034-DFRC.html.

[42] Palmer JM. Pioneer-Venus Solar Flux Radiometer. In: Wyman CL, editor., SPIE Proceedings - The International Society for Optical Engineering; 1979, p. 305–11. https://doi.org/10.1117/12.957427.

[43] Choi M. Using Pre-melted Phase Change Material to Keep Payload Warm without Power for Hours in Space. 10th International Energy Conversion Engineering Conference, Reston, Virigina: American Institute of Aeronautics and Astronautics; 2012, p. 1–10. https://doi.org/10.2514/6.2012-3894.

[44] Hasan A, McCormack SJ, Huang MJ, Norton B. Evaluation of phase change materials for thermal regulation enhancement of building integrated photovoltaics. Solar Energy 2010;84:1601–12. https://doi.org/10.1016/j.solener.2010.06.010.

[45] Hasan A, McCormack S, Huang M, Norton B. Energy and Cost Saving of a Photovoltaic-Phase Change Materials (PV-PCM) System through Temperature Regulation and Performance Enhancement of Photovoltaics. Energies 2014;7:1318–31. https://doi.org/10.3390/en7031318.

[46] Hasan A, McCormack SJ, Huang MJ, Sarwar J, Norton B. Increased photovoltaic performance through temperature regulation by phase change materials: Materials comparison in different climates. Solar Energy 2015;115:264–76. https://doi.org/10.1016/j.solener.2015.02.003.

[47] Machniewicz A, Knera D, Heim D. Effect of Transition Temperature on Efficiency of PV/PCM Panels. Energy Procedia 2015;78:1684–9. https://doi.org/10.1016/j.egypro.2015.11.257.

[48] Stropnik R, Stritih U. Increasing the efficiency of PV panel with the use of PCM. Renewable Energy 2016;97:671–9.

https://doi.org/10.1016/j.renene.2016.06.011.

[49] Hasan A, Sarwar J, Alnoman H, Abdelbaqi S. Yearly energy performance of a photovoltaic-phase change material (PV-PCM) system in hot climate. Solar Energy 2017;146:417–29. https://doi.org/10.1016/j.solener.2017.01.070.

[50] Lim J-H, Lee Y-S, Seong Y-B. Diurnal Thermal Behavior of Photovoltaic Panel with Phase Change Materials under Different Weather Conditions. Energies 2017;10:1983. https://doi.org/10.3390/en10121983.

[51] Luo Z, Huang Z, Xie N, Gao X, Xu T, Fang Y, et al. Numerical and experimental study on temperature control of solar panels with form-stable paraffin/expanded graphite composite PCM. Energy Conversion and Management 2017;149:416–23. https://doi.org/10.1016/j.enconman.2017.07.046.

[52] Huang MJ, Eames PC, Norton B, Hewitt NJ. Natural convection in an internally finned phase change material heat sink for the thermal management of photovoltaics. Solar Energy Materials and Solar Cells 2011;95:1598–603. https://doi.org/10.1016/j.solmat.2011.01.008.

[53] Atkin P, Farid MM. Improving the efficiency of photovoltaic cells using PCM infused graphite and aluminium fins. Solar Energy 2015;114:217–28. https://doi.org/10.1016/j.solener.2015.01.037.

[54] Bayrak F, Oztop HF, Selimefendigil F. Experimental study for the application

of different cooling techniques in photovoltaic (PV) panels. Energy Conversion and Management 2020;212:112789. https://doi.org/10.1016/j.enconman.2020.112789.

[55] Firoozzadeh M, Shiravi AH, Shafiee M. Thermodynamics assessment on cooling photovoltaic modules by phase change materials (PCMs) in critical operating temperature. Journal of Thermal Analysis and Calorimetry 2021;144:1239–51. https://doi.org/10.1007/s10973-020-09565-3.

[56] Khanna S, Reddy KS, Mallick TK. Optimization of finned solar photovoltaic phase change material (finned pv pcm) system. International Journal of Thermal Sciences 2018;130:313–22. https://doi.org/10.1016/j.ijthermalsci.2018.04.033.

[57] Bria A, Raillani B, Chaatouf D, Salhi M, Amraqui S, Mezrhab A. Effect of PCM thickness on the performance of the finned PV/PCM system. Materials Today: Proceedings 2022. https://doi.org/10.1016/j.matpr.2022.08.409.

[58] Duan J. The PCM-porous system used to cool the inclined PV panel. Renewable Energy 2021;180:1315–32. https://doi.org/10.1016/j.renene.2021.08.097.

[59] Abdulmunem AR, Samin PM, Rahman HA, Hussien HA, Ghazali H. A novel thermal regulation method for photovoltaic panels using porous metals filled with phase change material and nanoparticle additives. Journal of Energy Storage 2021;39:102621. https://doi.org/10.1016/j.est.2021.102621.

[60] Firoozzadeh M, Shiravi AH. Simultaneous use of porous medium and phase

change material as coolant of photovoltaic modules; thermodynamic analysis. Journal of Energy Storage 2022;54:105276. https://doi.org/10.1016/j.est.2022.105276.

[61] Sharaf M, Huzayyin AS, Yousef MS. Performance enhancement of photovoltaic cells using phase change material (PCM) in winter. Alexandria Engineering Journal 2022;61:4229–39. https://doi.org/10.1016/j.aej.2021.09.044.

[62] Rubitherm. RT25HC Data Sheet 2020.

[63] Firoozzadeh M, Shiravi AH, Shafiee M. Different methods of using phase change materials (PCMs) as coolant of photovoltaic modules: A review. Research Article Journal of Energy Management and Technology (JEMT) 2020;4:30.

[64] Firoozzadeh M, Shiravi AH. Simultaneous use of porous medium and phase change material as coolant of photovoltaic modules; thermodynamic analysis. Journal of Energy Storage 2022;54:105276. https://doi.org/10.1016/j.est.2022.105276.

[65] TommaTech. Polikristal 36p n.d.

[66] Rubitherm. RT25HC Data Sheet 2020.

[67] Rubitherm. RT35HC Data Sheet 2020.

[68] Aalco Metals. Aluminium Alloy 1050A H14 Sheet 2019.

[69] Evans DL, Florschuetz LW. Cost studies on terrestrial photovoltaic power systems with sunlight concentration. Solar Energy 1977;19:255–62. https://doi.org/10.1016/0038-092X(77)90068-8.

[70] Holman JP. Experimental Methods for Engineers. 2012.

APPENDICES

Appendix A: Photovoltaic Module Description

POLİKRİSTAL 36P

TOMMATECH GmbH

GERMAN-based company

- TT5-18P (5 Wp)
- TT10-36P (10 Wp)
- TT22-36P (22 Wp)
- TT42-36P (42 Wp)
- TT55-36P (55 Wp)
- TT85-36P (85 Wp)
- TT110-36P (110 Wp)
- TT170-36P (170 Wp)

12 YIL Malzeme ve İşçilik Garantisi

30 YIL Performans Garantisi

Yüksek Dönüşüm Verimliliği
Yüksek Panel Verimliliği Sayesinde, Yüksek Güç Çıkışını Garanti Eder.

Kendi Kendini Temizleyen ve Yansımayı Azaltan Cam
Cam Üzerindeki Özel Kaplama Yüzey Tozunu Azaltır.

Düşük Işınımda Yüksek Verimlilik
Sabah ve Bulutlu Hava Koşullarında Dahi Yüksek Panel Verimliliği

Mükemmel Dayanım Kapasitesi
2400 Pa Rüzgar Yükü, 5400 Pa Kar Yüküne Karşı Dayanım

0~+5Wp Pozitif Güç Toleransı

Kolay Kurulum

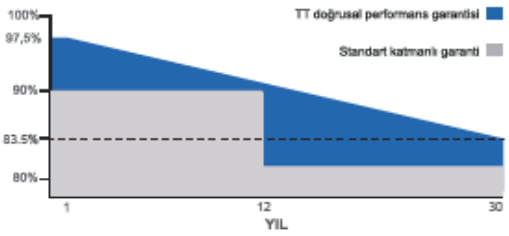

30 Yıl Performans Garantisi

12 Yıl Malzeme ve İşçilik Garantisi

IEC 61215
IEC 61730 - 1 IEC 61730 - 2
IEC 62716 IEC 61701

Tommatech GmbH - München / GERMANY

www.tommatech.de
info@tommatech.de

Model Tipi	TT5-18P	TT10-36P	TT22-36P	TT42-36P	TT55-36P	TT85-36P	TT110-36P	TT170-36P
Maksimum Güç (P_{max})	5 Wp	10 Wp	22 Wp	42 Wp	55 Wp	85 Wp	110 Wp	170 Wp
Maksimum Güç Gerilimi (V_{mp})	9,86	19,73	19,73	19,73	19,73	19,73	19,73	19,73
Maksimum Güç Akımı (I_{mp})	0,51	0,51	1,12	2,13	2,83	4,31	5,58	8,62
Açık Devre Gerilimi (V_{oc})	11,61	23,22	23,22	23,22	23,22	23,22	23,22	23,22
Kısa Devre Akımı (I_{sc})	0,54	0,54	1,19	2,26	3,00	4,51	5,81	9,02
Hücre Sayısı	18(2x9)	36(4x9)	36(4x9)	36(4x9)	36(4x9)	36(4x9)	36(4x9)	36(4x9)
Hücre Boyutu (mm)	20x78	20x78	39x78	39x157	52,25x157	78x157	97x157	157x157
Panel Boyutu (mm)	204x254x16	364x254x16	365x425x16	680x430x20	680x554x20	680x790x20	680x1025x25	680x1504x30
Ağırlık (kg)	0,68	1,13	1,9	3,32	4,2	5,87	7,53	11,7
Gerilim (v)	9V	12V	12V	12V	12V	12V	12V	12V
Çalışma Sıcaklığı Aralığı	-40 ~ +85°C							

MEKANİK ÖZELLİKLER

Solar Cam	3,2mm Düşük Demirli, Temperli Cam		
Çerçeve	Eloksal Kaplı Alüminyum		
Bağlantı Kutusu	IP65 (5-85 Wp)		
Bağlantı Kutusu	IP67 (110-170 Wp)		
Kablo	4mm²		
Kablo Boyu	55Wp 430mm	85Wp 475mm	170 Wp 1000mm

SICAKLIK KATSAYISI

Sıcaklık Katsayısı (Isc)	0.06%/°C
Sıcaklık Katsayısı (Voc)	-0.31%/°C
Sıcaklık Katsayısı (Pmax)	-0.38%/°C
Nominal Çalışma Hücre Sıcaklığı (NOCT)	45°C±2°C

FİZİKSEL ÖZELLİKLER

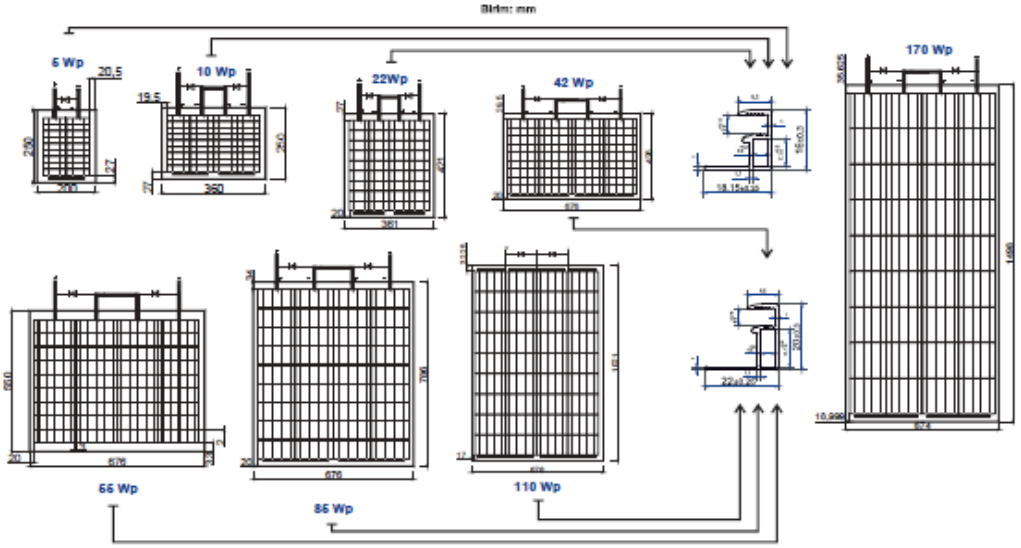

*Not: Elde edilen veriler; Standart Test Koşulları: 1000 W/m² güneş ışınımı, (AM 1.5) ve hücre sıcaklığı 25°C. Nominal Test Koşulları: 800 W/m² güneş ışınımı, ortam sıcaklığı 20°C, rüzgar hızı 1m/s. Tüm paneller için ölçüm belirsizliği %5'dir. Gerçek veriler yapılan sözleşmelere tabi olacaktır. Bu parametreler sadece referans amaçlıdır ve bu sözleşmelerin bir parçası değildir. Teknik özellikler, önceden haber verilmeksizin değiştirilebilir.

www.tommatech.de

Appendix B: Phase Change Material Descriptions

Data sheet

RUBITHERM

RT25HC

RUBITHERM® RT is a pure PCM, this heat storage material utilising the processes of phase change between solid and liquid (melting and congealing) to store and release large quantities of thermal energy at nearly constant temperature. The RUBITHERM® phase change materials (PCM's) provide a very effective means for storing heat and cold, even when limited volumes and low differences in operating temperature are applicable.

Properties for RT-line:
- high thermal energy storage capacity
- heat storage and release take place at relatively constant temperatures
- no supercooling effect, chemically inert
- long life product, with stable performance through the phase change cycles
- melting temperature range between -9 °C and 100 °C available

The most important data:	Typical Values	
Melting area	22-26 main peak: 25	[°C]
Congealing area	26-22 main peak: 25	[°C]
Heat storage capacity ± 7,5% Combination of latent and sensible heat in a temperatur range of 16°C to 31 °C.	230	[kJ/kg]*
	58	[Wh/kg]*
Specific heat capacity	2	[kJ/kg·K]
Density solid at 15°C	0,88	[kg/l]
Density liquid at 40°C	0,77	[kg/l]
Heat conductivity (both phases)	0,2	[W/(m·K)]
Volume expansion	12,5	[%]
Flash point	150	[°C]
Max. operation temperature	65	[°C]

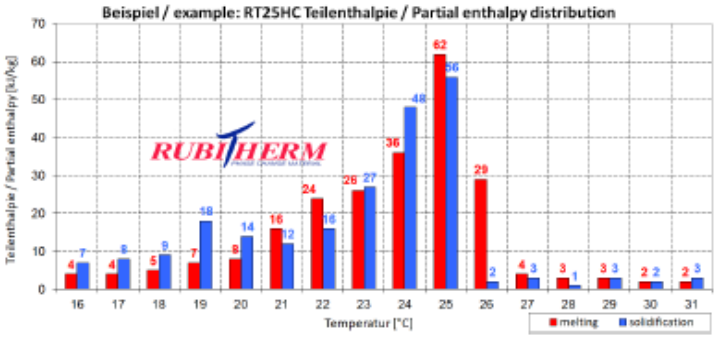

Rubitherm Technologies GmbH
Imhoffweg 6
D-12307 Berlin
phone: +49 (30) 7109622-0
E-Mail: info@rubitherm.com
Web: www.rubitherm.com

Version: 09.10.2020

*Measured with 3-layer-calorimeter.

Data sheet

RT35HC

RUBITHERM® RT is a pure PCM, this heat storage material utilising the processes of phase change between solid and liquid (melting and congealing) to store and release large quantities of thermal energy at nearly constant temperature.
The RUBITHERM® phase change materials (PCM's) provide a very effective means for storing heat and cold, even when limited volumes and low differences in operating temperature are applicable.

Properties for RT-line:
- **high thermal energy storage capacity**
- **heat storage and release take place at relatively constant temperatures**
- **no supercooling effect, chemically inert**
- **long life product, with stable performance through the phase change cycles**
- **melting temperature range between -9 °C and 100 °C available**

The most important data:	Typical Values	
Melting area	34-36 main peak: 35	[°C]
Congealing area	36-34 main peak: 35	[°C]
Heat storage capacity ± 7,5% Combination of latent and sensible heat in a temperatur range of 27°C to 42 °C.	240	[kJ/kg]*
	67	[Wh/kg]*
Specific heat capacity	2	[kJ/kg·K]
Density solid at 25°C	0,88	[kg/l]
Density liquid at 40°C	0,77	[kg/l]
Heat conductivity (both phases)	0,2	[W/(m·K)]
Volume expansion	12	[%]
Flash point	177	[°C]
Max. operation temperature	70	[°C]

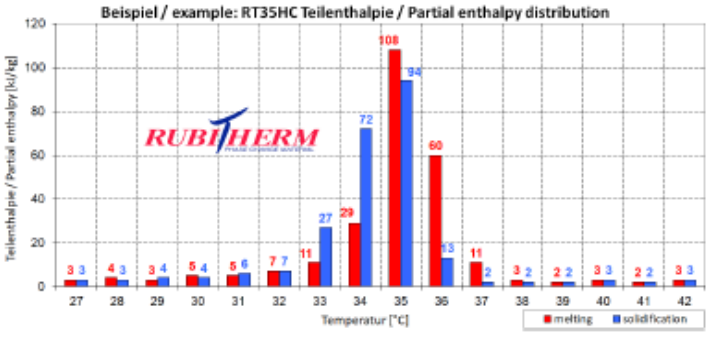

Rubitherm Technologies GmbH
Imhoffweg 6
D-12307 Berlin
phone: +49 (30) 7109622-0
E-Mail: info@rubitherm.com
Web: www.rubitherm.com

Version: 09.10.2020

*Measured with 3-layer-calorimeter.

Appendix C: Technical Drawings of Parts Manufactured

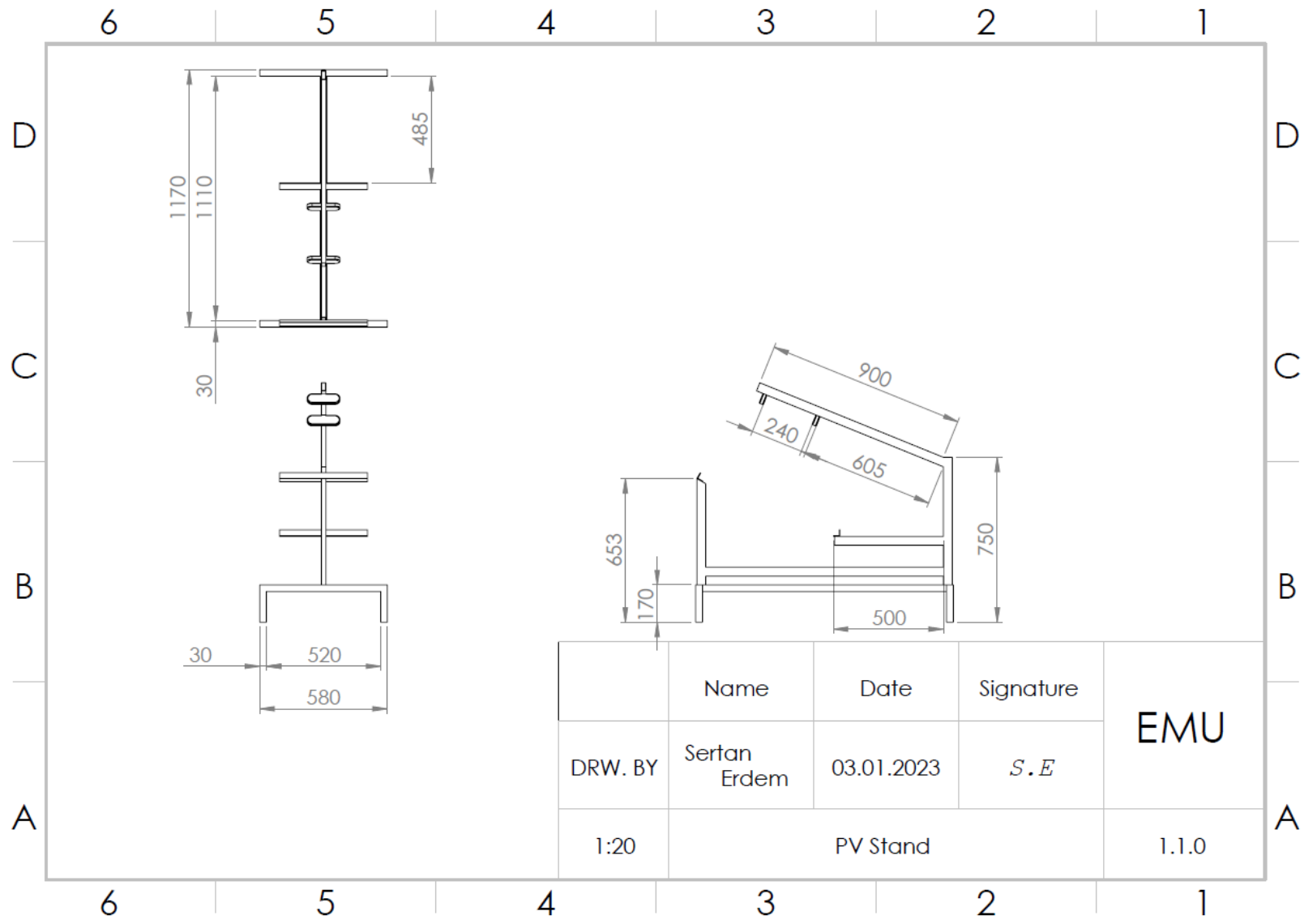
6
5
4
3
2
1
D
C
B
A
485
1170
1110
30
30
520
580
900
240
605
653
170
750
500
Name
Date
Signature
EMU
DRW. BY
Sertan Erdem
03.01.2023
S.E
1:20
PV Stand
1.1.0

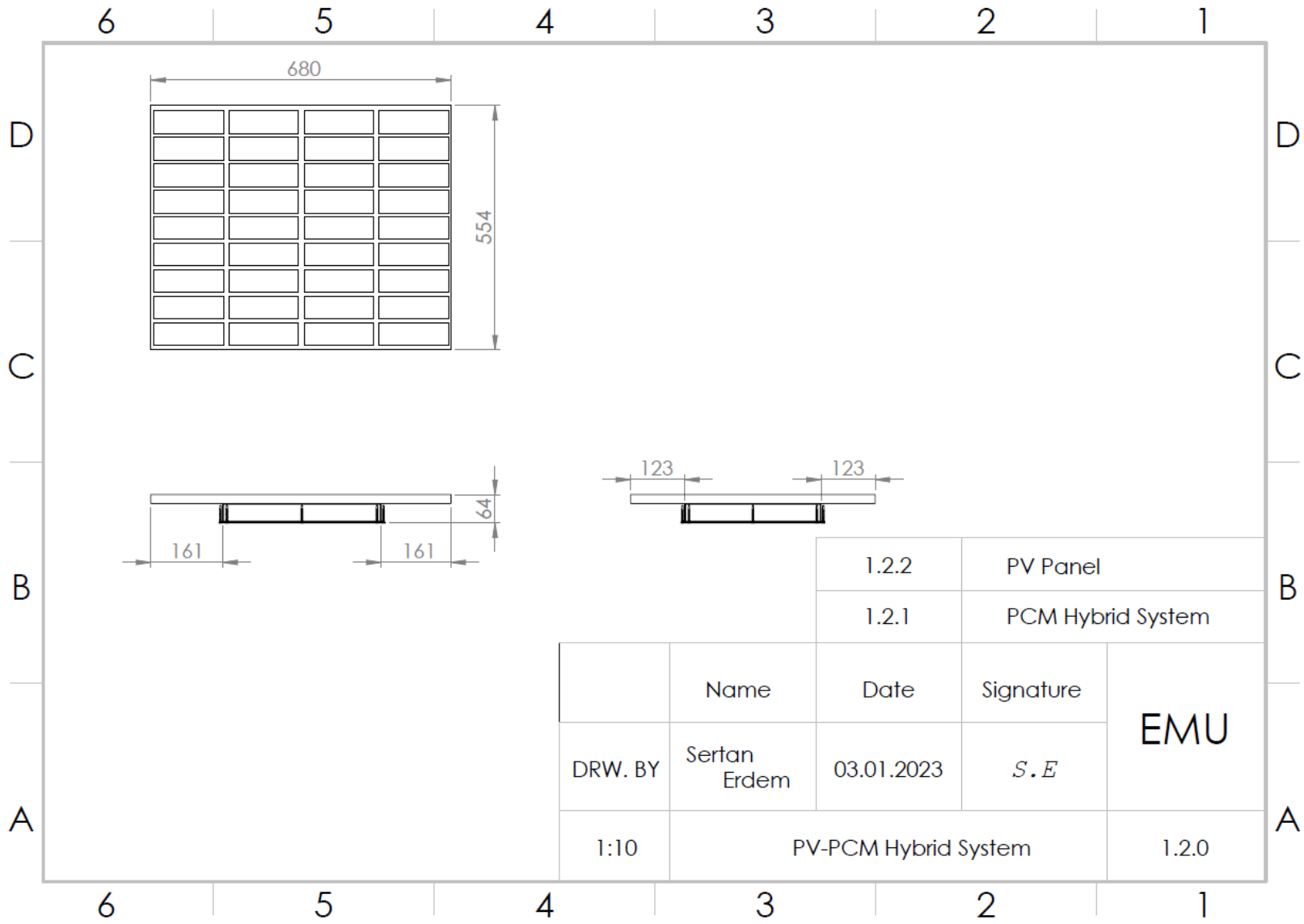
6
5
4
3
2
1
D
C
B
A
680
554
64
161
161
123
123
1.2.2
PV Panel
1.2.1
PCM Hybrid System
Name
Date
Signature
EMU
DRW. BY
Sertan Erdem
03.01.2023
S.E
1:10
PV-PCM Hybrid System
1.2.0

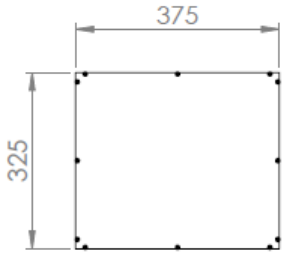

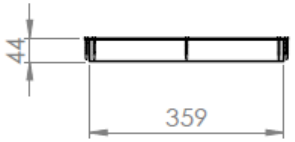

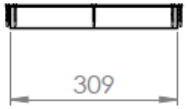

1.2.1.3	Top Cover		
1.2.1.2	Reservoir		
1.2.1b.1	Perforated Sheet		
1.2.1a.1	Fin		

	Name	Date	Signature	
DRW. BY	Sertan Erdem	03.01.2023	*S.E*	EMU
1:5	PCM-Hybrid System			1.2.1

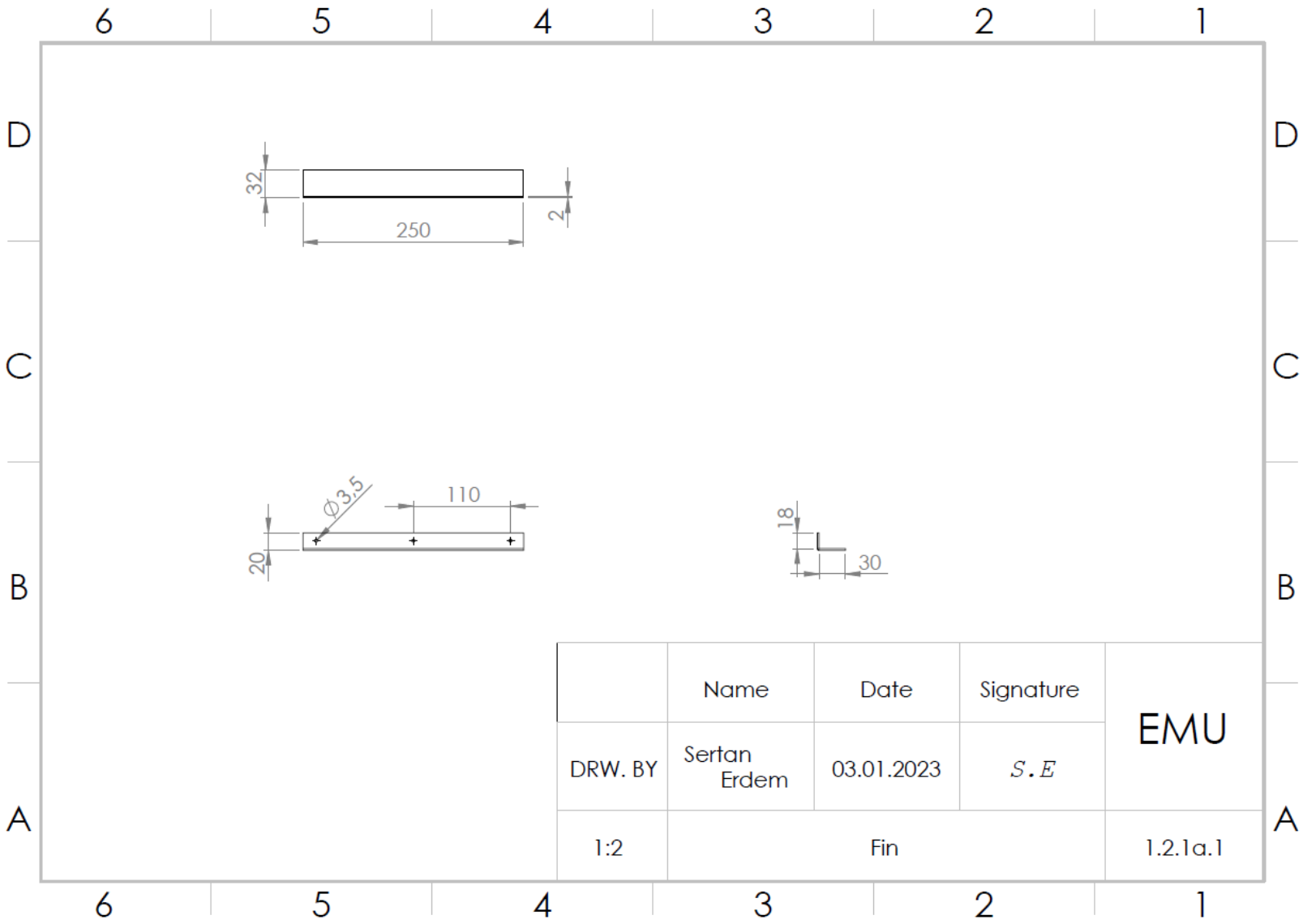

	Name	Date	Signature	EMU
DRW. BY	Sertan Erdem	03.01.2023	S.E	
1:2	Fin			1.2.1a.1

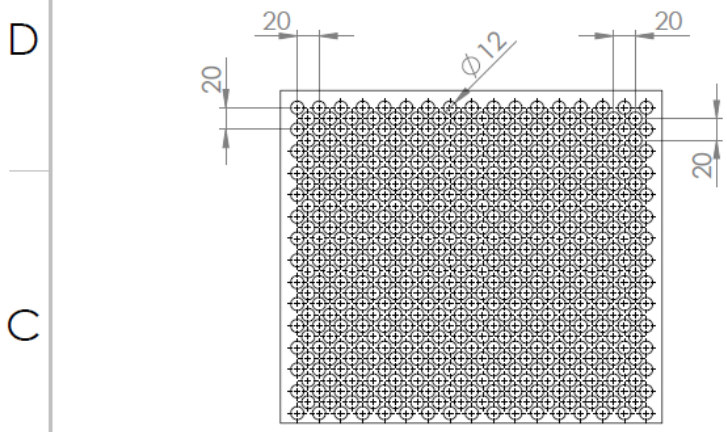

	Name	Date	Signature	EMU
DRW. BY	Sertan Erdem	03.01.2023	S.E	
1:5	Perforated Sheet			1.2.1b.1

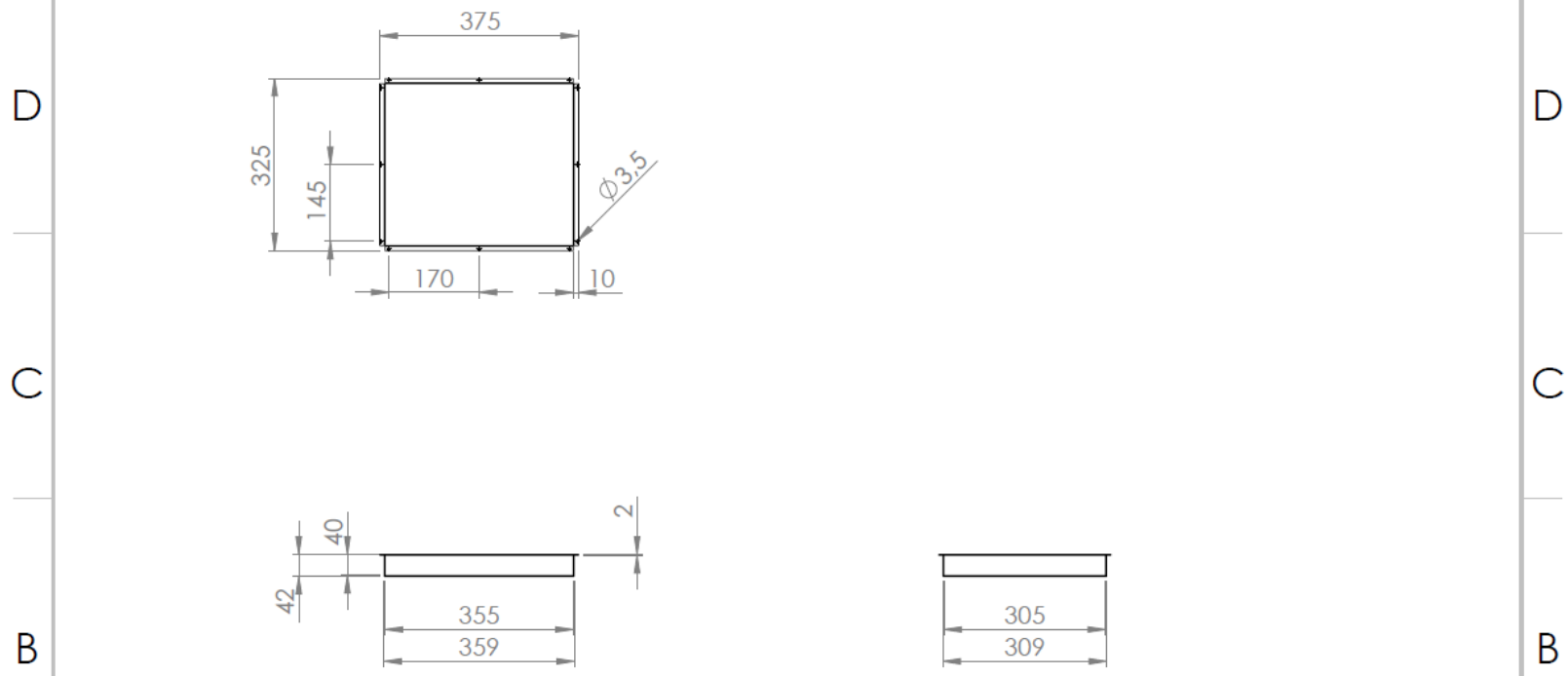

	Name	Date	Signature	EMU
DRW. BY	Sertan Erdem	03.01.2023	S.E	
1:5	Reservoir			1.2.1.2

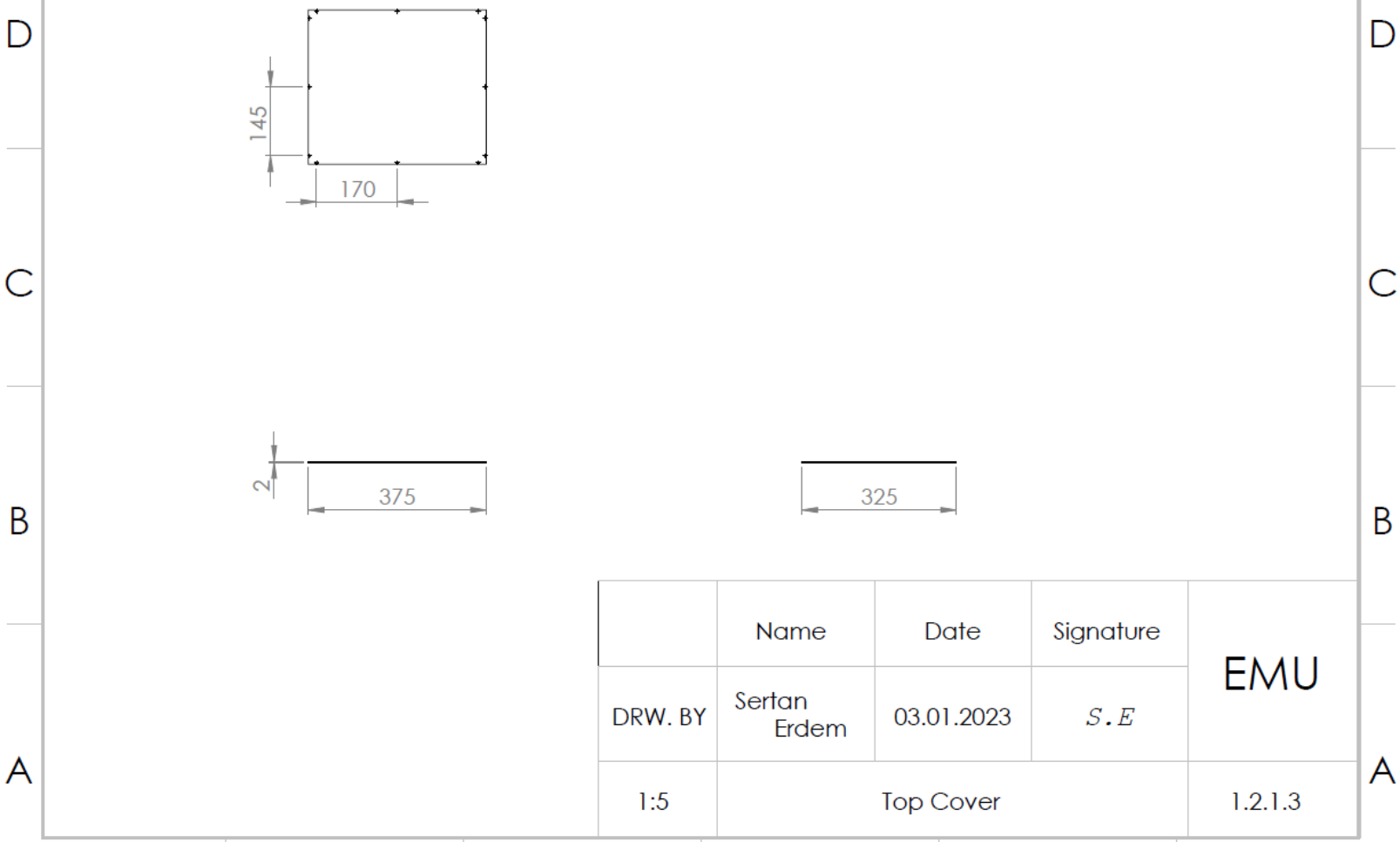
6
5
4
3
2
1
D
C
B
A
145
170
2
375
325
Name
Date
Signature
EMU
DRW. BY
Sertan Erdem
03.01.2023
S.E
1:5
Top Cover
1.2.1.3

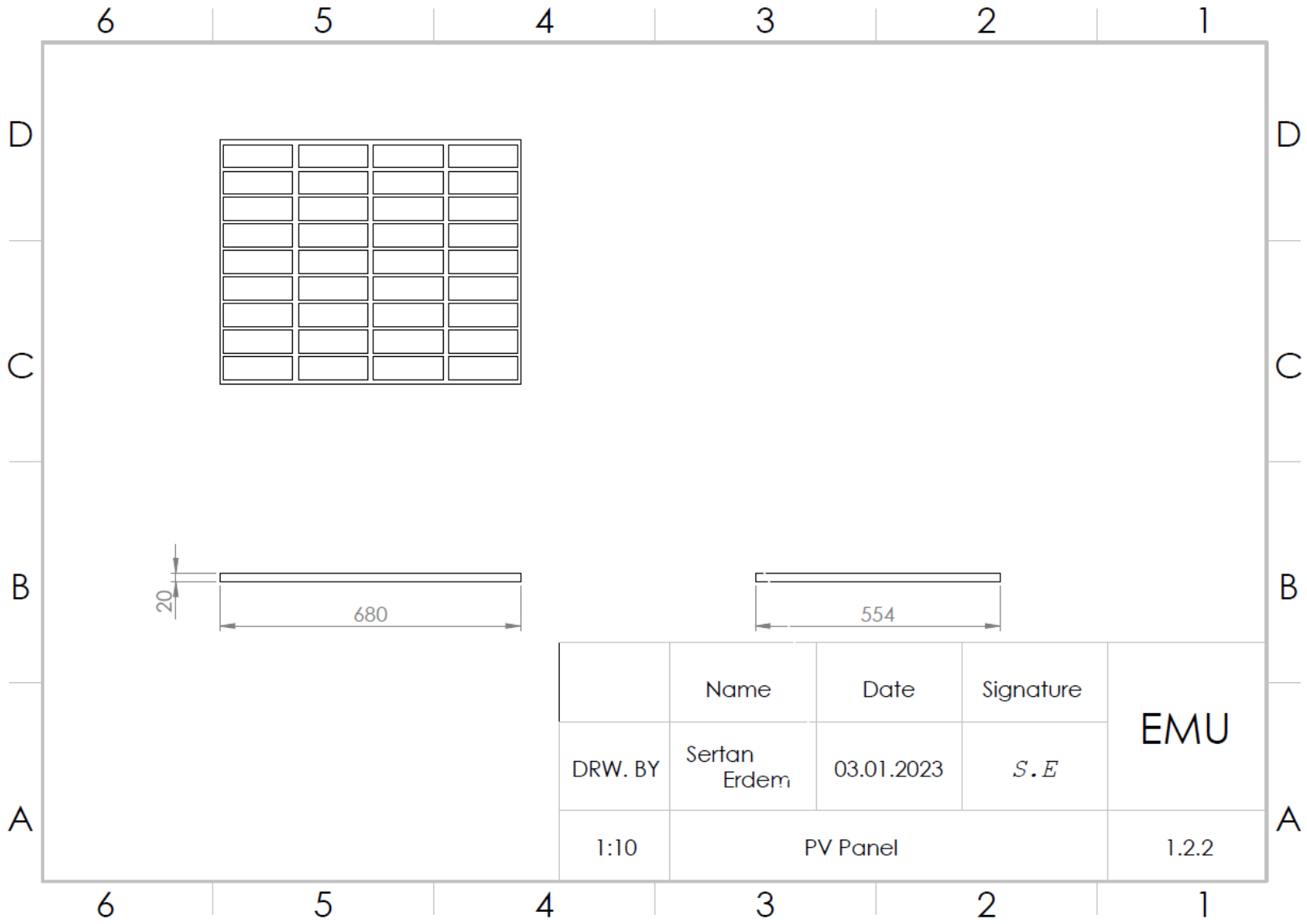
6
5
4
3
2
1
D
C
B
A
20
680
554
Name
Date
Signature
DRW. BY
Sertan Erdem
03.01.2023
S.E
EMU
1:10
PV Panel
1.2.2